Neuron

Membraneless condensates by Rapsn phase separation as a platform for neuromuscular junction formation

Highlights

- Rapsn phase-separates *in vitro,* in HEK293T cells and in muscles
- Rapsn co-condensates to recruit cargo proteins to membraneless compartments
- Rapsn condensates as a signaling platform
- Disease mutations impair rapsn condensates and co-condensates, and NMJ formation

Authors

Guanglin Xing, Hongyang Jing, Zheng Yu, Peng Chen, Hongsheng Wang, Wen-Cheng Xiong, Lin Mei

Correspondence

wen-cheng.xiong@case.edu (W.-C.X.), lin.mei@case.edu (L.M.)

In brief

Rapsn is critical for acetylcholine receptor (AChR) clustering and NMJ formation. Xing et al. show that Rapsn undergoes phase separation and that the resulting condensates recruit the AChR and signaling proteins to form membraneless compartments. These processes are compromised by congenital myasthenic syndrome mutations of Rapsn.

Xing et al., 2021, Neuron *109*, 1963–1978
June 16, 2021
https://doi.org/10.1016/j.neuron.2021.04.021

CellPress

Neuron

CellPress

Article

Membraneless condensates by Rapsn phase separation as a platform for neuromuscular junction formation

Guanglin Xing,[1] Hongyang Jing,[1] Zheng Yu,[1] Peng Chen,[1] Hongsheng Wang,[1] Wen-Cheng Xiong,[1,2,*] and Lin Mei[1,2,3,*]
[1]Department of Neurosciences, School of Medicine, Case Western Reserve University, 10900 Euclid Avenue, Cleveland, OH 44106, USA
[2]Louis Stokes Cleveland Veterans Affairs Medical Center, Cleveland, OH 44106, USA
[3]Lead contact
*Correspondence: wen-cheng.xiong@case.edu (W.-C.X.), lin.mei@case.edu (L.M.)
https://doi.org/10.1016/j.neuron.2021.04.021

SUMMARY

Our daily life depends on muscle contraction, a process that is controlled by the neuromuscular junction (NMJ). However, the mechanisms of NMJ assembly remain unclear. Here we show that Rapsn, a protein critical for NMJ formation, undergoes liquid-liquid phase separation (LLPS) and condensates into liquid-like assemblies. Such assemblies can recruit acetylcholine receptors (AChRs), cytoskeletal proteins, and signaling proteins for postsynaptic differentiation. Rapsn LLPS requires multivalent binding of tetratricopeptide repeats (TPRs) and is increased by Musk signaling. The capacity of Rapsn to condensate and co-condensate with interaction proteins is compromised by mutations of congenital myasthenic syndromes (CMSs). NMJ formation is impaired in mutant mice carrying a CMS-associated, LLPS-deficient mutation. These results reveal a critical role of Rapsn LLPS in forming a synaptic semi-membraneless compartment for NMJ formation.

INTRODUCTION

Muscle contraction enables us to breathe, drink and eat, walk, and move body parts. The control of it requires proper function of the neuromuscular junction (NMJ), a cholinergic synapse between motor nerve terminals and muscle fibers (Li et al., 2018; Sanes and Lichtman, 1999; Tintignac et al., 2015; Wu et al., 2010). Action potentials stimulate motor nerve terminals to release acetylcholine (ACh), which activates ACh receptors (AChRs) to depolarize muscle fibers and triggers calcium release from the sarcoplasmic reticulum to initiate muscle contraction. AChRs are packed at the postjunctional membrane at a concentration of 10,000–20,000/μm^2 (Fambrough et al., 1973; Fertuck and Salpeter, 1976). Also enriched beneath the postjunctional membrane are a plethora of cytoplasmic signaling proteins and cytoskeletal proteins that are critical for induction and/or maintenance of AChR expression at the NMJ (Li et al., 2018; Wu et al., 2010). Reduced density or impaired function of the AChR is implicated in neurological disorders, including myasthenia gravis, amyotrophic lateral sclerosis, and congenital myasthenic syndromes (CMSs) (Cappello and Francolini, 2017; Engel et al., 2015; Gilhus et al., 2019; Li et al., 2018). Unlike innumerable synapses in the brain that are formed onto dendrites and somata of a neuron, the NMJ is positioned in the middle of a muscle fiber, occupying ~0.01%–0.1% of the surface. How the AChR becomes concentrated has interested neuroscientists of many generations. Prior to innervation by motor nerves, muscle fibers develop nascent, aneural AChR clusters (Lin et al., 2001; Yang et al., 2000, 2001) that mark a central region of muscle fibers to attract incoming motor nerve axons (Flanagan-Steet et al., 2005; Liu et al., 2008). After innervation, nerve terminals release agrin, which binds to LRP4 to activate Musk in muscle cells (DeChiara et al., 1996; Glass et al., 1996; Jennings et al., 1993; Kim et al., 2008; McMahan, 1990; Zhang et al., 2008); the ensuing signaling leads to formation of large AChR clusters. At the same time, activation of muscle fibers by ACh disperses extrasynaptic AChR clusters (Lin et al., 2005; Misgeld et al., 2005; Shi et al., 2012). This complex interplay requires that the necessary signaling proteins overcome the enormous cytoplasmic volume to be concentrated beneath the postjunctional membrane (i.e., into a membraneless compartment that is not enclosed by lipid membranes), a process that is not well understood.

Rapsn was identified as a co-purifying protein of the AChR from the electric organ of the torpedo ray (Neubig and Cohen, 1979; Sobel et al., 1978). It plays a critical role in NMJ formation and maintenance. Rapsn-null mutant mice fail to form aneural AChR clusters and NMJs (Gautam et al., 1995; Li et al., 2016; Xing et al., 2019). Numerous mutations have been identified in individuals with CMS (Milone et al., 2009). In heterologous cells, Rapsn alone is able to form puncta and recruit co-transfected AChRs into the puncta (Froehner et al., 1990; Li et al., 2016; Phillips et al., 1991); Rapsn mutant myotubes fail to form AChR clusters without altering AChR protein levels (Fuhrer et al., 1999; Xing et al., 2019). As a classic adaptor protein, Rapsn is believed to anchor the AChR by binding to cytoskeleton-associated proteins such as β-dystroglycan, α-actinin, and MACF1 (Bartoli et al., 2001; Dobbins et al., 2008; Oury et al., 2019). In addition, Rapsn can interact with and engage signaling proteins

to regulate NMJ formation (Li et al., 2018; Wu et al., 2010; Xing et al., 2020). For example, its interaction with calpain can counteract the inhibitory effect of muscle activation on AChR clustering (Chen et al., 2007). Recent studies suggest that Rapsn may serve as an enzyme whose activity is necessary for NMJ formation (Li et al., 2016; Xing et al., 2019). The mechanisms of how Rapsn initiates and maintains AChR clustering remain unclear.

Phase separation is key for the formation of membraneless signaling complexes and supramolecular assemblies (Boeynaems et al., 2018; Chen et al., 2020; Shin and Brangwynne, 2017; Wu et al., 2020). Via a process called liquid-liquid phase separation (LLPS), signaling as well as structural proteins undergo phase transition into liquid-like condensates that exist stably in a liquid milieu. Such membraneless, coherent structures contribute to spatiotemporal regulation of gene expression (Boija et al., 2018), assembly of the cytoskeleton and tight junctions (Beutel et al., 2019; Hernández-Vega et al., 2017; Schwayer et al., 2019; Woodruff et al., 2017), regulation of enzyme activities (Guo et al., 2020; Zhu et al., 2020), and autophagic degradation (Wilfling et al., 2020; Zhang et al., 2018). Aberrant LLPS or liquid-solid phase transition has been implicated in neurodegenerative disorders (Alberti and Dormann, 2019; Hofweber et al., 2018; Molliex et al., 2015; Murakami et al., 2015). Recently, LLPS has been implicated in active zone formation, synaptic vesicle clustering, and postsynaptic density (PSD) formation (Bai et al., 2021; Feng et al., 2019; McDonald et al., 2020; Milovanovic et al., 2018; Wu et al., 2019; Zeng et al., 2016, 2018, 2019). The postsynaptic proteins PSD-95, SynGAP, Shank, GKAP, and Homer do not condensate individually, but, when mixed, PSD-95 and SynGAP undergo LLPS. Shank, GKAP, and Homer, when mixed, were also able to condensate and co-condensate with PSD-95 and SynGAP (Feng et al., 2019; Zeng et al., 2016, 2018, 2019), suggesting phase separation as a possible mechanism of PSD formation.

Here we show that Rapsn is able to condensate into liquid-like compartments *in vitro*, in HEK293T cells and in muscles via phase separation. Rapsn co-condensates with AChR subunits as well as cytoskeletal proteins, demonstrating that, via LLPS, Rapsn serves as a vehicle to recruit different cargo proteins. Remarkably, the capacity of Rapsn to phase-separate and co-condensate with cargo proteins is compromised by CMS mutations, providing genetic evidence of an *in vivo* role of LLPS. Rapsn does not contain an intrinsically disordered region that is required for LLPS (Boeynaems et al., 2018; Shin and Brangwynne, 2017). We show that Rapsn LLPS is driven by the TPR (tetratricopeptide repeat)-containing domain, which possesses multivalent binding properties and is promoted by Musk-mediated tyrosine phosphorylation. These results suggest that Rapsn LLPS into a semi-membraneless compartment underlies NMJ formation and maintenance.

RESULTS

Phase separation of Rapsn into condensates *in vitro*

To determine whether Rapsn can phase-separate into liquid-like condensates, enhanced green fluorescent protein (EGFP)-tagged Rapsn (Rapsn-EGFP) was purified from transfected HEK293T cells (Figure 1A). Time-lapse microscopy analysis indicated that Rapsn-EGFP was able to spontaneously form spherical, condensed droplets in physiological buffer (Figures 1A and 1B; Video S1). Quantitatively, droplet numbers and sizes increased gradually over time (Figures 1C and 1D) and in a concentration-dependent manner because more and larger droplets were formed with 5 μM Rapsn-EGFP than with 1 μM (Figures 1B-1D). In contrast, as a control, no droplets were detectable with EGFP even at 10 μM (Figure 1B). To further eliminate a possible role of EGFP, we generated recombinant Rapsn without the EGFP tag (Figure S1A) and labeled it with a red dye (Mix-n-Stain CF555, CF555-Rapsn) (Zeng et al., 2018). As shown in Figures S1B–S1D, CF555-Rapsn could also form droplets. These results indicated that Rapsn was able to phase-separate into condensates.

To demonstrate that Rapsn indeed condensates into droplets from an aqueous phase, Rapsn solution was subjected to centrifugation (14,000 × *g*, 15 min) (Figure 1E), and the amounts of Rapsn in the condensed phase and aqueous phase were visualized by silver staining. Rapsn-EGFP and Rapsn were detectable in the pellets after centrifugation (Figures 1F and S1E), also in a concentration-dependent manner (Figures 1G and S1F). In addition, Rapsn LLPS was dependent on salt concentration and inhibited in the presence of 500 mM NaCl. At 150 mM NaCl, 30% of Rapsn was detected in the condensed phase, and when LLPS was inhibited in the presence of 500 mM NaCl, Rapsn was barely detectable in the condensed phase (Figures 1G and S1F). These results provide evidence that Rapsn phase-separates into a condensed phase directly from an aqueous phase.

Condensed droplets of Rapsn had liquid properties. First, two droplets could fuse upon contact (Figure 1H; Video S1). Second, when a droplet was photobleached, the fluorescence was able to recover rapidly, with a time constant of $t_{1/2}$ (the time at which half of the fluorescence recovers) = 23 s (Figures 1I and 1K; Video S2), suggesting a dynamic exchange of Rapsn between aqueous and condensed phases. This notion is supported by the observation that, when a region of a droplet was photobleached, fluorescence recovery in the bleached area occurred at a faster rate ($t_{1/2}$ = 16 s) (Figures 1J and 1L; Video S3). These results indicate an extensive exchange of Rapsn proteins between condensates and surrounding buffer and within the condensates.

Rapsn phase separation into subcellular compartments in HEK293T cells, myotubes, and muscle

Rapsn is known to form puncta in heterologous cells (Froehner et al., 1990; Phillips et al., 1991). To examine whether these puncta are phase-separated membraneless compartments, HEK293T cells were transfected with Rapsn-EGFP and examined 12 h after transfection. Confocal analysis by collapsed z stack images showed that Rapsn-EGFP formed puncta in HEK293T cells (Figure 2A), consistent with previous work (Li et al., 2016; Xing et al., 2019). Single-plane analysis at the middle of cells indicated that these puncta were attached to the plasma membrane (Figure 2B), presumably because of myristoylation (Frail et al., 1988). Rapsn puncta were spherical or elliptical in HEK293T cells, as revealed by 3D reconstruction analysis (Figures 2C and 2D). As shown in Video S4, Rapsn puncta changed size and shape

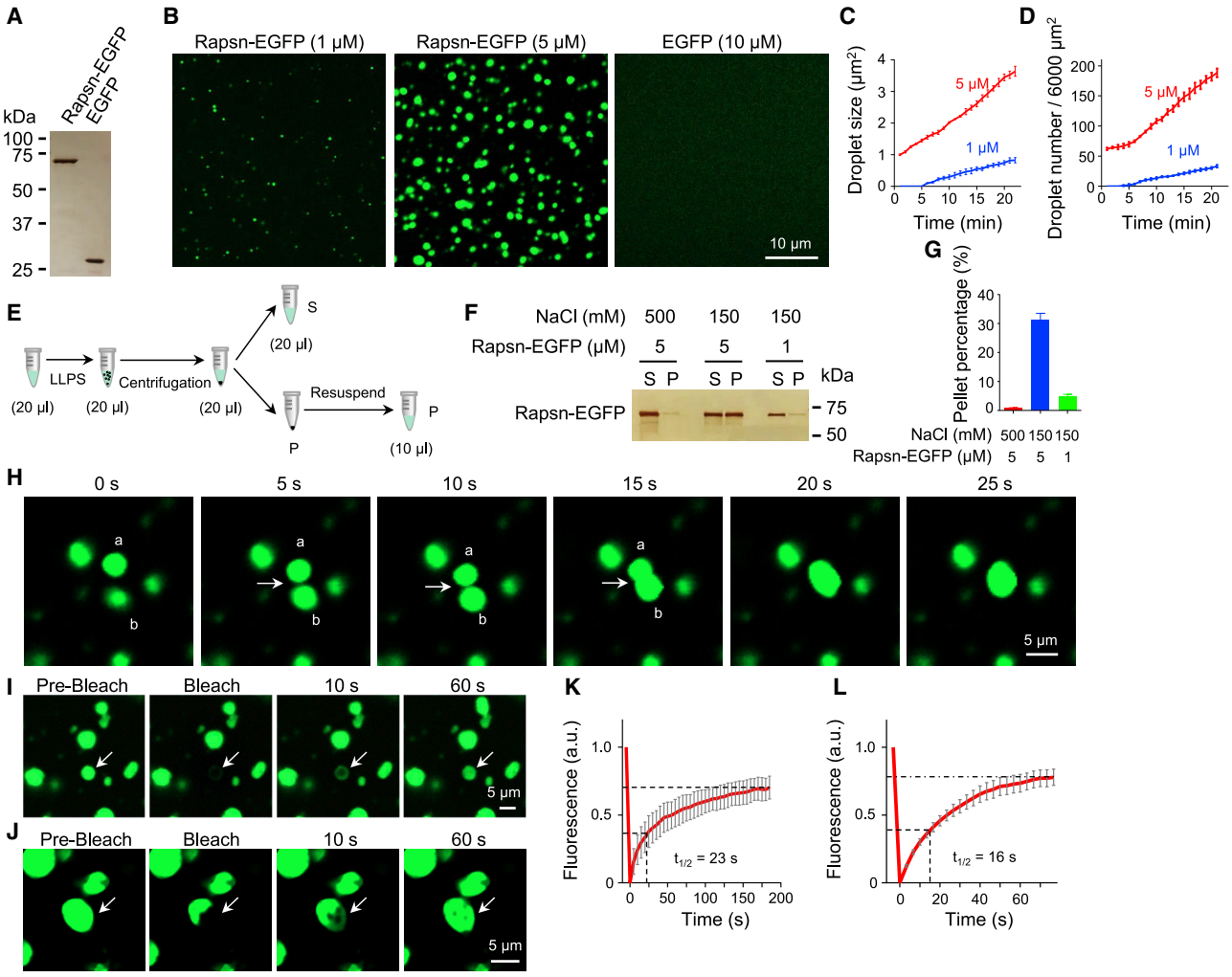

Figure 1. LLPS of Rapsn-EGFP into condensates *in vitro*

(A–D) LLPS of Rapsn-EGFP, but not EGFP, into condensed droplets in a concentration-dependent manner.

(A) Silver staining showing Rapsn-EGFP and EGFP.

(B) Rapsn-EGFP, but not EGFP, was able to phase-separate into condensed droplets. Rapsn-EGFP (1 μM and 5 μM) and EGFP (10 μM) were diluted into physiological buffer, and after 20 min, representative images were acquired.

(C and D) Quantification of droplet size and number at the indicated times.

(E) Schematic showing separation of the condensed phase from the aqueous phase by centrifugation.

(F) High salt and lower protein concentrations reduced the amount of Rapsn in pellets. Shown is representative silver staining.

(G) Quantification of Rapsn-EGFP in pellets in (F).

(H) Fusion of two Rapsn-EGFP droplets.

(I–L) Rapsn-EGFP in condensed droplets exchanged extensively with the surrounding aqueous phase or within droplets. Shown is fluorescence recovery after photobleaching (FRAP) analysis of a Rapsn-EGFP droplet (I) and part of a droplet (J) and quantification of fluorescence recovery in (I) and (J) (K and L).

Data are shown as mean ± SEM; n ≥ 3. See also Figure S1.

constantly; adjacent puncta could coalesce into one upon contact (Figure 2E; Video S4, red arrow). In addition, the fluorescence of photobleached puncta could recover rapidly within seconds ($t_{1/2}$ = 16 s) (Figures 2F and 2G; Video S4, white arrow). When a part of a punctum was photobleached, the fluorescence recovered at a faster rate ($t_{1/2}$ = 12 s) (Figures 2H and 2I). Similar results were observed in HEK293T cells expressing mCherry-tagged Rapsn (Figures S2A–S2C). These results indicate that Rapsn puncta in HEK293T cells are membraneless subcellular compartments formed by LLPS and that the exchange of Rapsn between the compartments and the environment and within the compartment is dynamic.

To determine whether Rapsn LLPS occurs in myotubes, we performed time-lapse imaging. To avoid potential non-specific effects of Rapsn overexpression, which prevents formation of large AChR clusters (Han et al., 1999; Yoshihara and Hall, 1993), Rapsn-EGFP was transfected in *Rapsn*$^{-/-}$ myoblasts (Fuhrer et al., 1999). The resulting myotubes were examined for

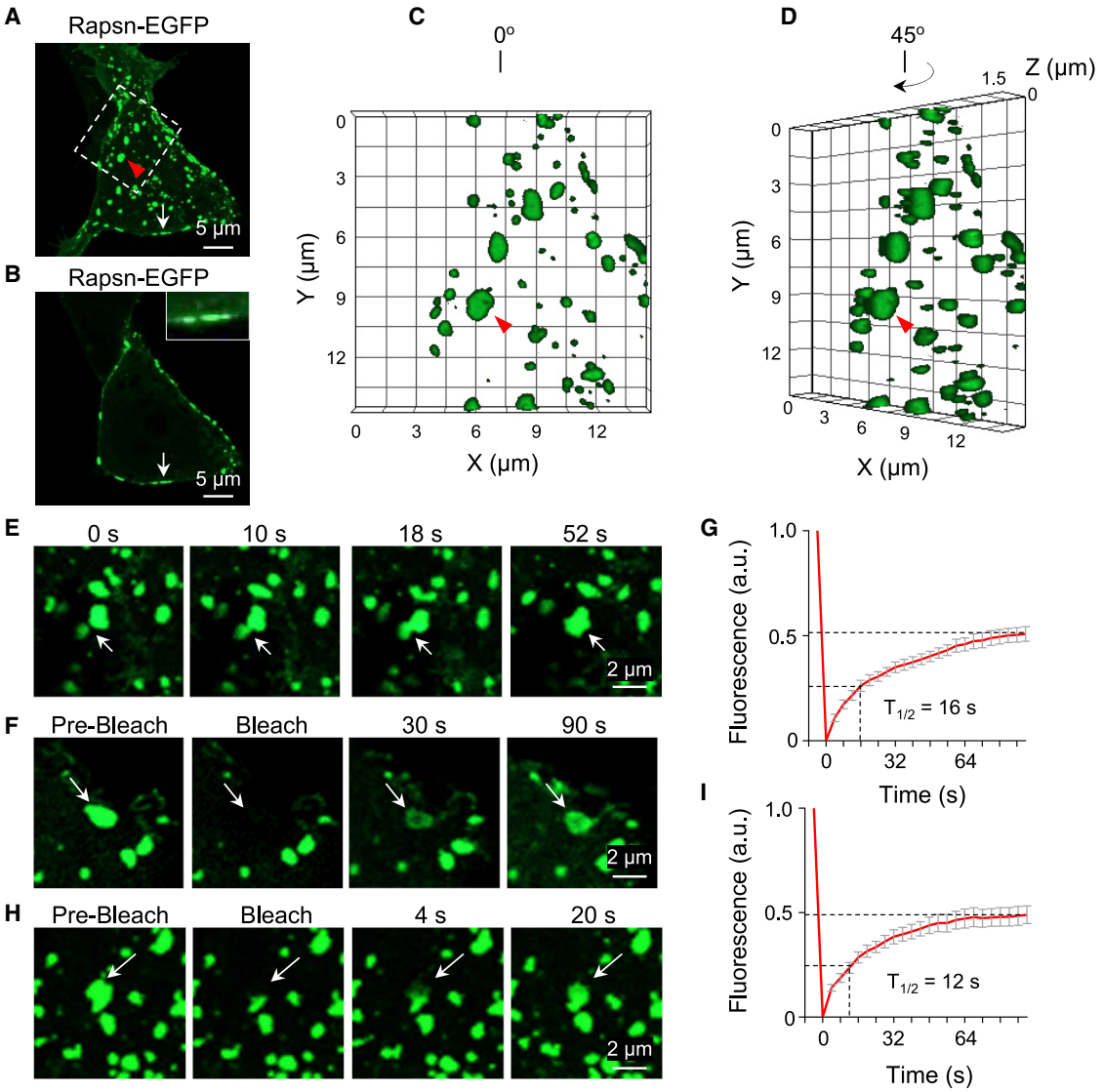

Figure 2. Rapsn LLPS into liquid-like compartments in HEK293T cells

(A–D) Formation of membrane-attached Rapsn-EGFP puncta in transfected HEK293T cells.

(A) Representative 3D projection image showing circular or oval Rapsn-EGFP puncta.

(B) Single-panel image showing membrane-attached Rapsn-EGFP puncta.

(C) High-magnification image showing the highlighted region in (A).

(D) View of the image in (C) at a different angle. White arrow, membrane-attached puncta; red triangle, the same punctum as in (A), (C), and (D).

(E) Fusion of two Rapsn-EGFP puncta in HEK293T cells.

(F–I) Dynamic exchange of Rapsn-EGFP between puncta and the surrounding milieu and within puncta in HEK293T cells.

(F and H) FRAP analysis of a Rapsn-EGFP punctum (F) and quantification of fluorescence recovery (H).

(G and I) FRAP analysis of part of a punctum (G) and quantification of fluorescence recovery (I).

Data are shown as mean ± SEM; n ≥ 3. See also Figure S2.

Rapsn-EGFP clusters. As shown in Figure 3A, in the absence of agrin, small Rapsn aggregates fused to form a large cluster within minutes. When part of a spontaneous cluster was photobleached, the fluorescence recovered quickly (Figures 3B and 3C; Video S5), suggesting that the clusters have liquid-like properties. Next we treated myotubes with agrin and examined agrin-induced clusters of Rapsn-EGFP. They grew by fusing small aggregates (Figure 3D). When partially photobleached, the fluorescence recovered within minutes (Figures 3E and 3F; Video S6). When a cluster was photobleached in its entirety, the fluorescence could also recover, albeit at a slower rate (Figures 3G and 3H; Video S7). These observations support the notion that Rapsn forms membraneless subcellular compartments via LLPS in myotubes.

Finally, we determined whether Rapsn LLPS occurs in live muscle fibers. Rapsn-EGFP was electroporated *in vivo* into

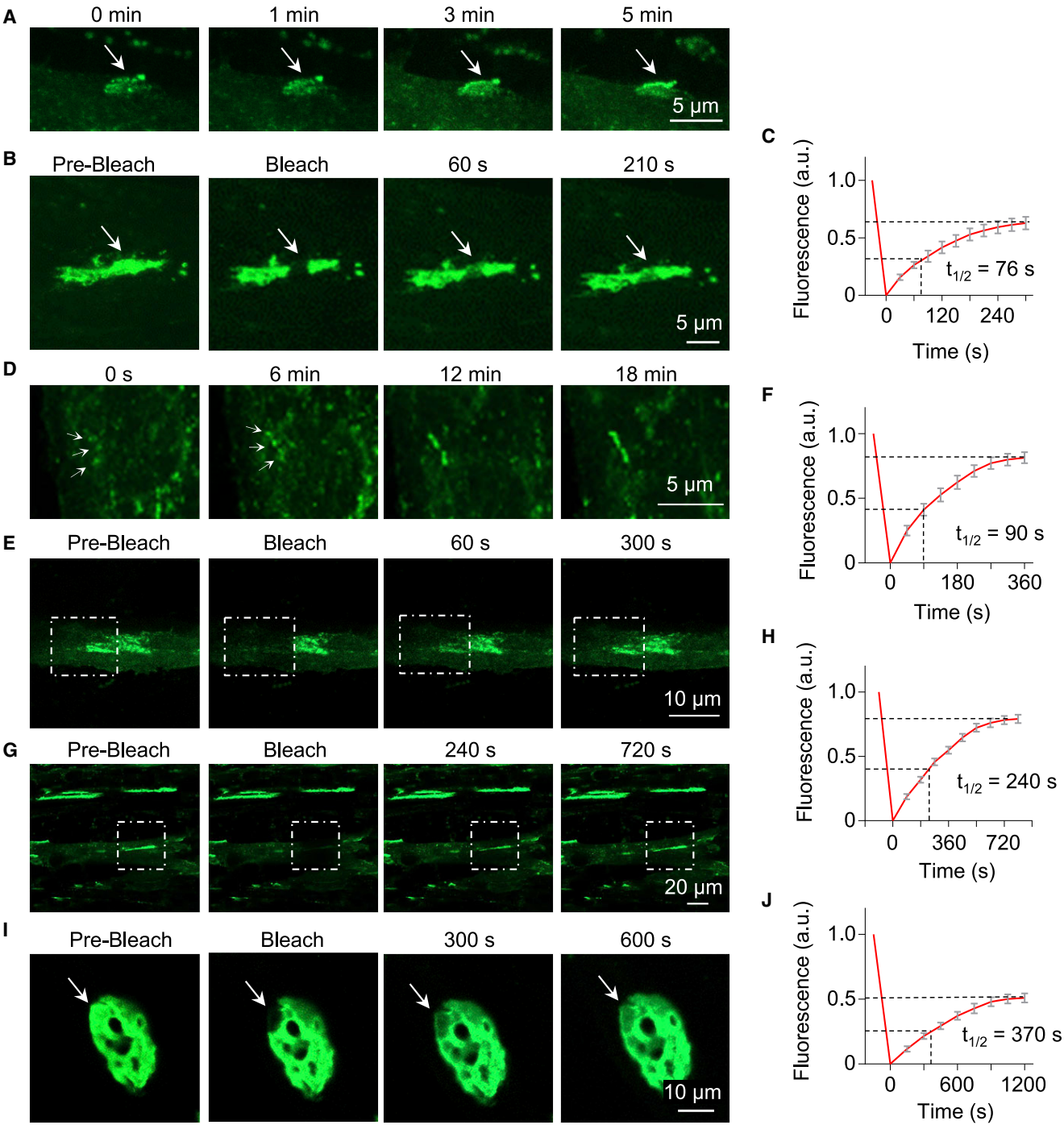

Figure 3. Rapsn LLPS into liquid-like compartments in myotubes and muscles

(A) Fusion of small spontaneous Rapsn-EGFP aggregates into large continuous clusters in myotubes. Arrow, cluster during fusion.
(B) Dynamic property of Rapsn-EGFP protein within spontaneous clusters.
(C) Quantification of fluorescence recovery in (B).
(D) Fusion of agrin-induced Rapsn-EGFP clusters in myotubes.
(E–H) Dynamic exchange of Rapsn-EGFP between clusters and the surrounding milieu and within clusters in myotubes.
(E and F) FRAP analysis of an agrin-induced Rapsn-EGFP cluster (E) and quantification of fluorescence recovery (F).
(G and H) FRAP analysis of part of a cluster (G) and quantification of fluorescence recovery (H).
(I and J) Dynamic property of Rapsn-EGFP in living muscles.
Data are shown as mean ± SEM; n ≥ 3.

tibialis anterior (TA) muscles on post-natal day 10 (P10). Muscles were isolated at P22 in oxygenated Ringer's solution and examined for *in vivo* EGFP clusters. As shown in Figures 3I and 3J, there was fast recovery of fluorescence of the photobleached area of Rapsn-EGFP clusters in live muscles. These results from HEK293T cells, myotubes, and muscles demonstrate that Rapsn-EGFP clusters are dynamic and support a role of Rapsn LLPS in NMJ development. It is interesting that the FRAP recovery rate of Rapsn-EGFP was slower in myotubes and muscle than that in HEK293T cells and that the Rapsn localization pattern in myotubes and muscle is quite different from that in HEK293T cells. This may be because Rapsn condensates in muscles as well as myotubes recruit muscle- or myotube-specific cytoskeletal components or other components that may constrain Rapsn. Moreover, during cluster or synapse development, Rapsn condensates may transition to a solid phase, a phenomenon that has been observed in the active-zone proteins ELKS-1 and SYD-2 (McDonald et al., 2020).

Multivalent binding of TPRs is critical for Rapsn LLPS

LLPS can be mediated by proteins with intrinsically disordered regions (Milovanovic et al., 2018). However, Rapsn does not have an intrinsically disordered domain (IUPred2A; https://iupred2a.elte.hu). Alternatively, LLPS can occur via multi-protein complexes, such as those formed by PSD95 and SynGAP (Zeng et al., 2016) and RIM/RIM-BP (Wu et al., 2019). However, Rapsn itself is sufficient for LLPS. Rapsn has multiple TPR domains, a common motif for protein-protein interaction (Perez-Riba and Itzhaki, 2019). Because two to three TPRs can form a concave groove for interaction (Perez-Riba and Itzhaki, 2019), and because Rapsn has seven TPRs, we posited that the TPR region of Rapsn may possess multiple interaction motifs. To test this hypothesis, we first generated recombinant proteins containing two or three TPR domains: TPR1–2, TPR3–4, TPR5–7, and domains containing CC (Coiled-Coil) and RING (Really Interesting New Gene), named CC-RING (Figure 4A), and examined their ability to bind Rapsn. In cells co-transfected with Rapsn-Myc, as shown in Figure 4B, Rapsn-EGFP was detected in the immunocomplex precipitated by anti-Myc beads. Rapsn-EGFP was not detected in cells that were not co-transfected with Rapsn-Myc (Figure 4B), indicating the specificity of the interaction. These results suggest that the Rapsn proteins were able to self-associate, in agreement with previous work (Li et al., 2016; Ramarao et al., 2001; Xing et al., 2019). Interestingly, Rapsn-Myc could also co-precipitate TPR1–2, TPR3–4, and TPR5–7 but not CC-RING (Figure 4B), indicating that TPR1–2, TPR3–4, and TPR5–7, but not CC-RING, bind with full-length Rapsn. To determine whether these TPR combinations bind to each other, HEK293T cells were co-transfected with a Myc-tagged TPR protein and EGFP-tagged Rapsn or a truncation mutant. Subsequent co-immunoprecipitation assays indicated that TPR1–2-Myc (Figure 4C), TRP3–4-Myc (Figure 4D), and TPR5–7-Myc (Figure 4E) could bind to full-length Rapsn and each of the three TPR proteins. In contrast, CC-RING-Myc failed to interact with full-length Rapsn or any of the TPR motifs (Figure 4F). These results suggest that two or more TPR motifs were able to form a binding motif for Rapsn and self-association. To further test this hypothesis, we generated additional TPR combinations: TPR2–3, TPR4–5, TPR5–6, and TPR6–7 (Figure S3A). As shown in Figure S3B, TPR2–3, TPR4–5, and TPR5–6, but not TPR6–7, could bind with full-length Rapsn. Moreover, these combinations could interact with one another (Figures S3C, S3D, and S3F). However, TPR6–7 did not interact with full-length Rapsn or any of the TPR combination (Figure S3E). These results suggest that Rapsn contains multiple self-interaction binding sites via various combinations of TPR motifs, revealing a potential molecular mechanism of Rapsn LLPS.

Next, we determined whether TPR-containing proteins alone or in combination undergo LLPS *in vitro*. As shown in Figures 4G and 4H, TPR1–7 was able to condensate to form droplets. The droplet sizes and numbers of TPR1–7-EGFP were comparable with those of full-length Rapsn-EGFP (Figures 4I and 4J), suggesting that TPR1–7 was sufficient for phase separation. This notion was supported by centrifugation assays, where similar amounts of TPR1–7 and full-length Rapsn were detected in the condensed phase (Figures 4K and 4L). In contrast, CC-RING failed to form detectable droplets or condensate into pellets (Figures 4H, 4K, and 4L), indicating a necessary role of TPR1–7 in Rapsn LLPS. TPR1–2, TPR3–4, TPR5–7, and TPR1–4 were not able to form droplets or condensate into pellets (Figures 4H–4L), although each of them was able to interact with full-length Rapsn. These results indicate that Rapsn LLPS requires the multivalent binding of the TPR region.

Recruitment of cargo proteins into Rapsn condensates

After finding that Rapsn phase-separated into membraneless compartments in cells (Figures 2 and 3), we hypothesized that Rapsn LLPS may serve as a vehicle to carry interaction or cargo proteins into its condensates. First, we generated glutathione S-transferase (GST) fusion proteins containing intracellular regions (loop 3/4) between the third and fourth transmembrane domains of the AChR-α and -β subunits, which are required for Rapsn interaction (Lee et al., 2009). The resulting GST fusion proteins, referred to as AChR-α and AChR-β hereafter, were purified (Figure S4A) and labeled with CF555. AChR-α or AChR-β alone was unable to phase-separate into droplets (Figure S4B); however, when mixed with equimolar Rapsn-EGFP, they were enriched in Rapsn droplets (Figures 5A–5C), suggesting recruitment of AChR-α or AChR-β by Rapsn LLPS. Consistently, AChR-α or AChR-β alone could not be detected in the condensed phase but could be detected when mixed with Rapsn (Figures S5C–S5F). As a negative control, GST was unable to be enriched into Rapsn droplets and could not form condensed pellets when mixed with Rapsn-EGFP (Figures 5B, 5C, S5A, and S5B), suggesting specificity of Rapsn-mediated recruitment.

Rapsn has been shown to associate with intracellular proteins that regulate the cytoskeleton or are involved in signaling transduction (Xing et al., 2020). Next we determined whether these proteins could be recruited into Rapsn condensates. We focused on proteins that directly interact with Rapsn, such as β-dystroglycan (Bartoli et al., 2001), α-actinin (Dobbins et al., 2008), MACF1 (Antolik et al., 2007; Oury et al., 2019), and calpain (Chen et al., 2007) (Figure 5A). The respective recombinant proteins were purified and labeled with CF555 (Figure S4A). They did not form condensates alone (Figure S4B) but were detectable in

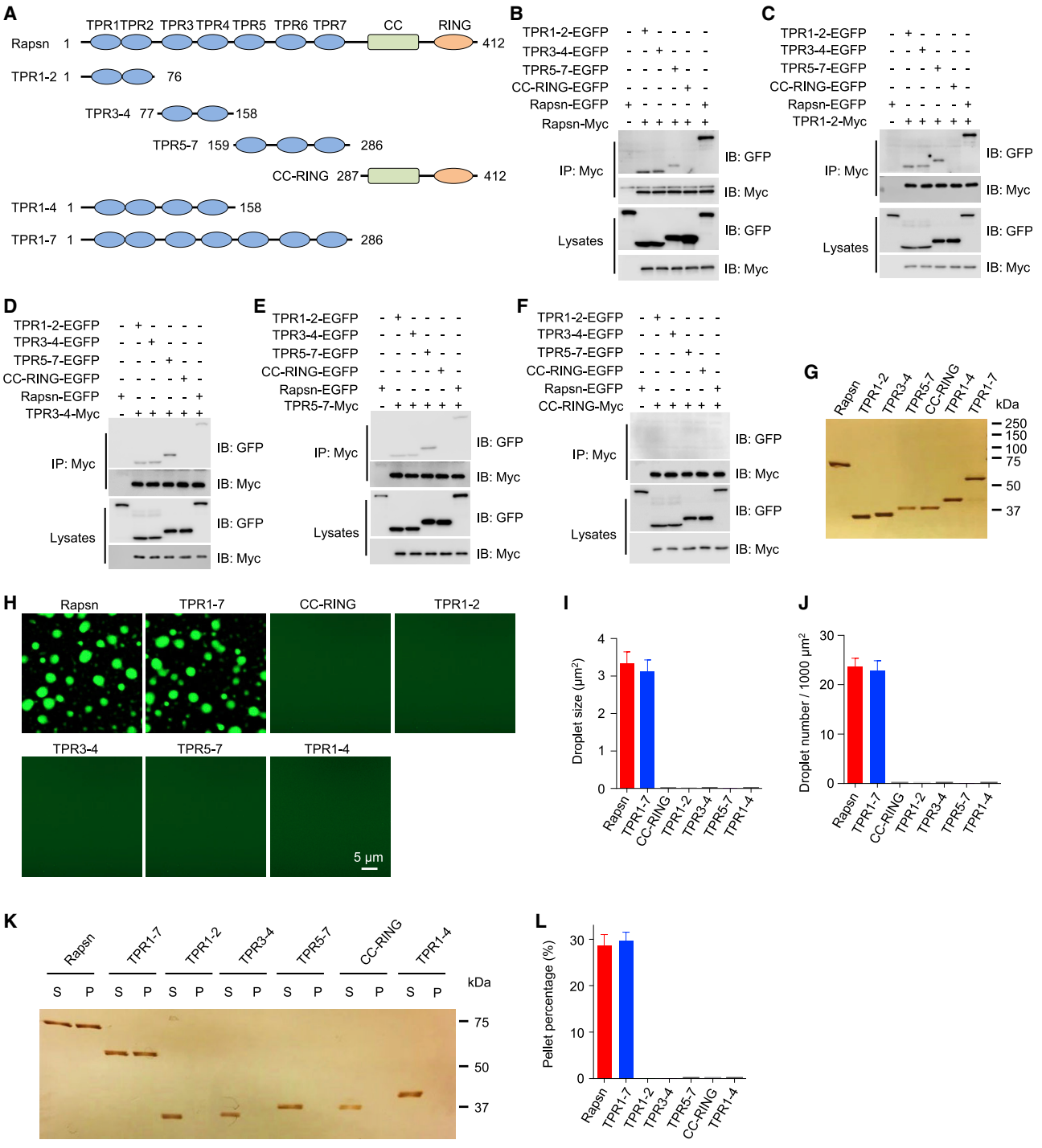

Figure 4. Multivalent binding of TPR domains for Rapsn LLPS

(A) Schematic domain structure of Rapsn and truncation mutants.

(B) Binding of Rapsn with TPR1–2, TPR3–4, TPR5–7, and full-length Rapsn but not CC-RING.

(C–F) TPR1–2 (C), TPR3–4 (D), and TPR5–7 (E), but not CC-RING (F), were able to self-interact and bind each other.

(G) Silver staining showing purified EGFP-tagged full-length and truncated Rapsn proteins.

(H) LLPS of TPR1–7 and full-length Rapsn but not CC-RING, TPR1–2, TPR3–4, TPR5–7, and TPR1–4.

(I and J) Quantification of droplet size (I) and number (J) in (H).

(legend continued on next page)

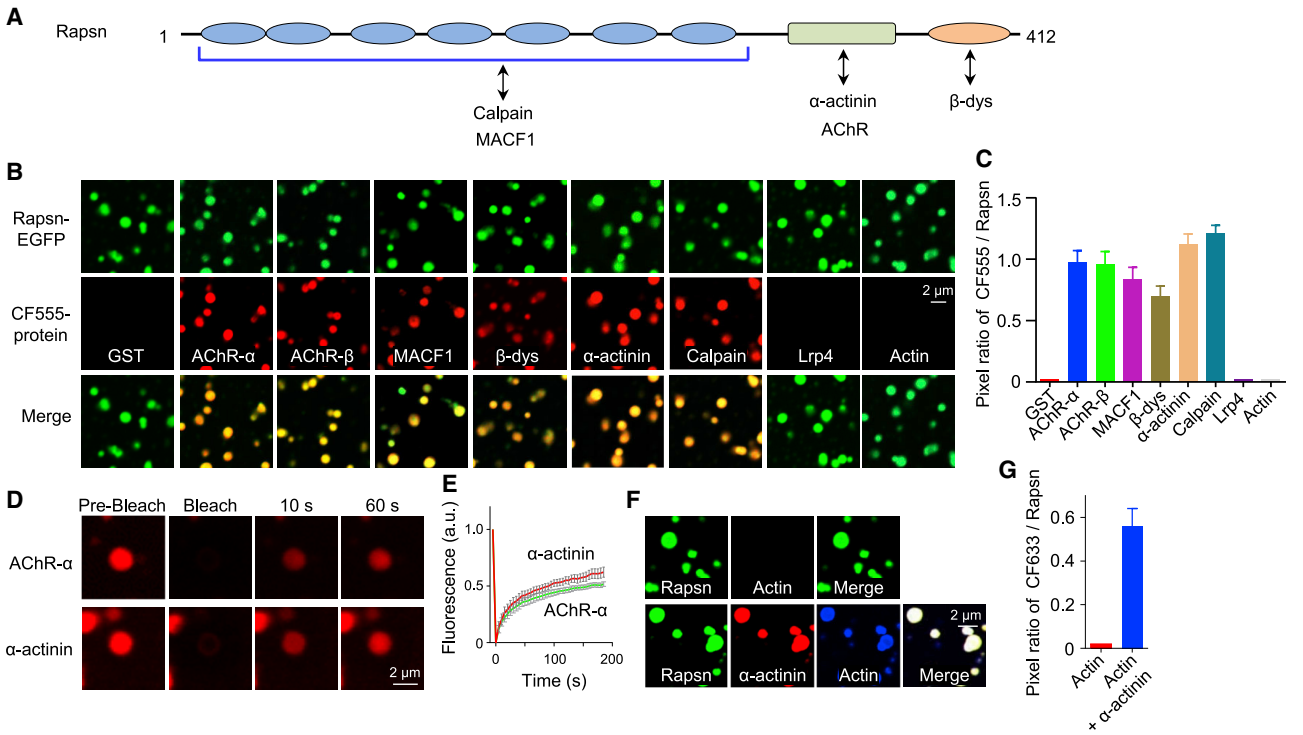

Figure 5. Recruitment of cargo proteins into Rapsn condensates

(A) Schematic domain structure of Rapsn and interaction proteins.

(B and C) AChR-α, AChR-β, MACF1, β-dystroglycan, α-actinin, or calpain, but not GST, LRP4, or actin, were recruited into Rapsn LLPS-mediated condensates.

(D) FRAP analysis of AChR-α and α-actinin enriched in Rapsn droplets, showing dynamic protein exchange.

(E) Quantification of fluorescence recovery of AChR-α and α-actinin in (D).

(F) Recruitment of actin into Rapsn condensed droplets in the presence of α-actinin.

(G) Quantification of the pixel ratio of CF633/Rapsn-EGFP in (F).

Data were shown as mean ± SEM; n ≥ 3. See also Figures S4 and S5.

Rapsn droplets (Figures 5B and 5C). In agreement, they were detected in the condensed phase when mixed with Rapsn but not alone (Figures S5G–S5N). These results suggest that Rapsn LLPS could enrich these interaction proteins into condensates. When CF555-AChR-α or α-actinin in Rapsn condensates was photobleached, the fluorescence recovered rapidly (Figures 5D and 5E), indicating that cargo proteins in Rapsn condensates are dynamic and exhibit rapid protein exchange between condensates and the surrounding buffer.

Co-immunoprecipitation evidence indicates that Rapsn associates with actin in electric organs in animals and in muscle cells (Li et al., 2016; Walker et al., 1984). However, CF555- or CF633-labeled actin was not detectable in Rapsn droplets or in the condensed phase (Figures 5B, 5C, 5F, 5G, S5Q, and S5R), perhaps because actin does not interact with Rapsn directly. Interestingly, in the presence of α-actinin, a protein that directly interacts with actin (Sjöblom et al., 2008), CF633-labeled actin was detectable in Rapsn droplets (Figures 5F and 5G), indicating that Rapsn may be able to recruit partners of its interaction proteins. Consistently, LRP4 was not detectable in Rapsn droplets and the condensed phase (Figures 5B, 5C, S5O, and S5P), although it was present in Rapsn aggregates in myotubes (Figure S5S), suggesting that LRP4 may be recruited indirectly into Rapsn aggregates.

Promotion of Rapsn LLPS by Musk signaling

Rapsn becomes tyrosine phosphorylated, which is necessary for aggregation and AChR clustering by agrin (Xing et al., 2019, 2020). Therefore, we determined whether Rapsn LLPS is regulated by tyrosine phosphorylation. First, Rapsn-EGFP was purified from transfected HEK293T cells, where it is tyrosine phosphorylated (Lee et al., 2008; Xing et al., 2019; Figure 6A). Treatment with lambda phosphatase (PP) reduced the phospho-tyrosine level of Rapsn (Figure 6A) and its ability to condensate (Figures 6B–6E), suggesting a potential regulation by tyrosine phosphorylation. In contrast, Src, a proto-oncogene

(K) Representative silver staining image showing that the WT and TPR1–7, but not TPR1–2, TPR3–4, TPR5–7, CC-RING, and TPR1–4, were able to condensate into pellets after centrifugation.

(L) Quantification of the percentage of proteins in pellets in (K).

Data are shown as mean ± SEM; n ≥ 3. See also Figure S3.

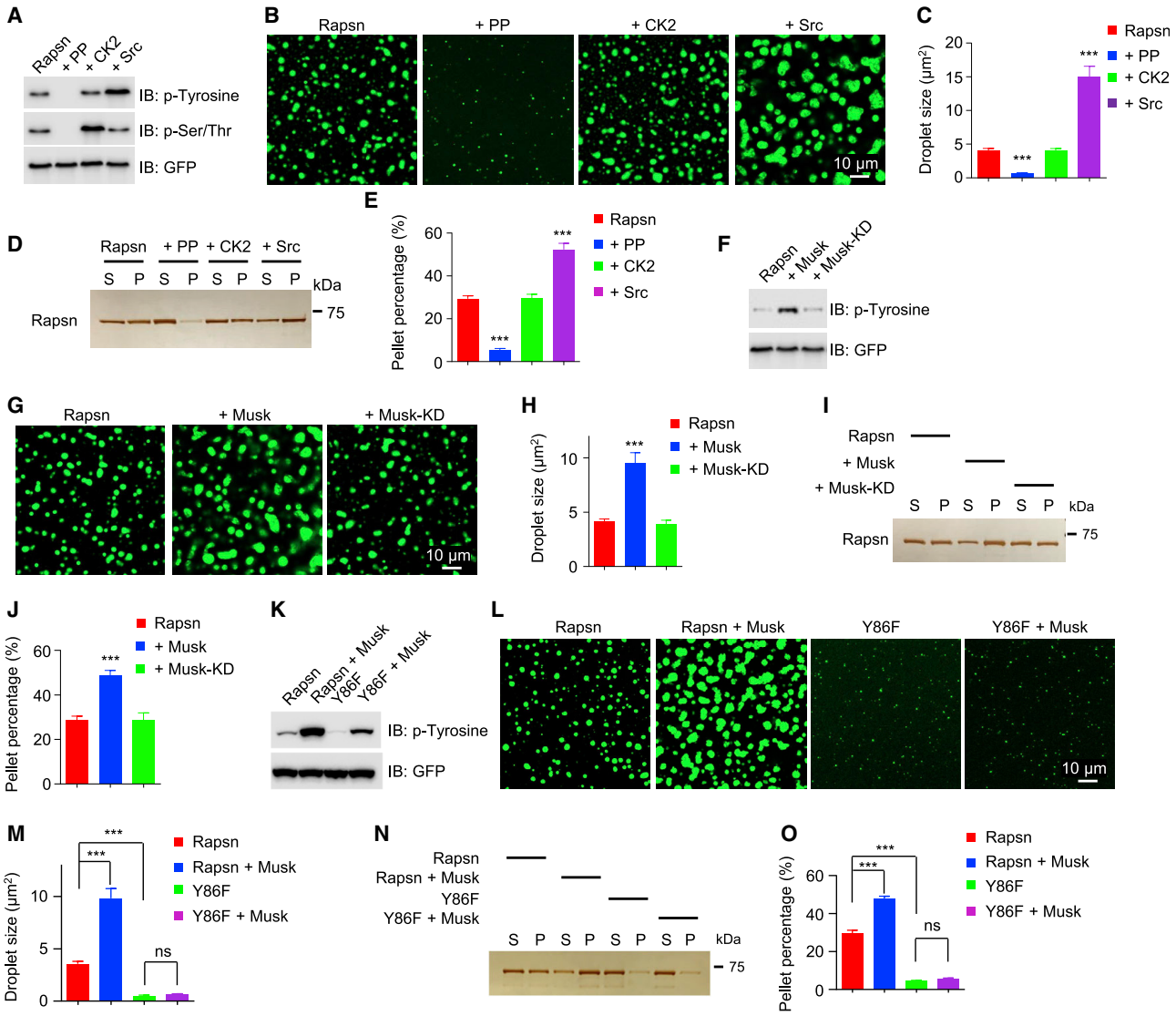

Figure 6. Promotion of Rapsn LLPS by Musk signaling

(A–E) Promotion of Rapsn LLPS by tyrosine phosphorylation. Rapsn-EGFP was treated with PP, CK2, or Src.

(A) Phosphorylation levels of Rapsn-EGFP.

(B and C) PP reduces and Src increases droplet formation.

(B) Representative blots.

(C) Quantitative data. ***$p < 0.001$, one-way ANOVA.

(D and E) PP reduces and Src increases Rapsn in pellets.

(D) Representative silver staining.

(E) Quantitative data. ***$p < 0.001$, one-way ANOVA.

(F–J) Enhanced Rapsn LLPS by Musk-induced tyrosine phosphorylation. Rapsn-EGFP was purified from HEK293T cells cotransfected with Musk or Musk-KD.

(F) Tyrosine phosphorylation of Rapsn.

(G and H) Increased droplet formation by Musk cotransfection. ***$p < 0.001$, one-way ANOVA.

(I and J) Increased Rapsn in pellets by Musk cotransfection. ***$p < 0.001$, one-way ANOVA.

(K–O) Reduced Rapsn LLPS by Y86F mutation. Rapsn or Y86F-EGFP was transfected into HEK293T cells alone or with Musk and purified for LLPS.

(K) Tyrosine phosphorylation of Rapsn.

(L) Representative images of droplets.

(M) Quantification of droplet size in (L). ***$p < 0.001$, one-way ANOVA.

(N) Reduced Y86F Rapsn in pellets.

(O) Quantitative data in (M). ***$p < 0.001$, one-way ANOVA.

Data are shown as mean ± SEM; $n \geq 3$.

tyrosine-protein kinase, increased the phospho-tyrosine of Rapsn (Figure 6A) and LLPS (droplet formation and condensation into pellets) (Figures 6B–6E). Because PP also reduced phospho-serine/threonine (Figure 6A), we determined whether serine/threonine phosphorylation was involved in Rapsn LLPS. Rapsn was incubated with casein kinase 2 (CK2), a serine/threonine kinase that binds to Rapsn and has been implicated in NMJ formation (Cheusova et al., 2006; Eiber et al., 2019; Herrmann et al., 2015), which increased the phospho-serine/threonine of Rapsn (Figure 6A). However, it had little effect on Rapsn droplet formation and condensation into pellets (Figures 6B–6E). These results suggest that Rapsn LLPS is promoted by tyrosine phosphorylation.

To examine whether Rapsn LLPS is regulated by Musk-induced tyrosine phosphorylation, we co-transfected Rapsn-EGFP with Musk into HEK293T cells. The co-transfection increased tyrosine phosphorylation of Rapsn compared with Rapsn-EGFP alone (Figure 6F), consistent with previous work (Lee et al., 2008; Xing et al., 2019). In parallel, Rapsn LLPS was increased (Figures 6G–6J). This effect was not observed with Rapsn from HEK293T cells co-transfected with kinase-dead Musk mutant (Musk-KD) (Figures 6F–6J). Previously, we showed that Y86 of Rapsn becomes tyrosine phosphorylated and its mutation, Y86F, reduces phosphorylation and self-association (Xing et al., 2019; Figure 6K). Interestingly, the droplet size and level of Y86F in condensed phase were reduced compared with WT Rapsn (Figures 6L–6O). In addition, the Y86F mutation inhibited Musk-promoted Rapsn LLPS (both droplet formation and condensation into pellets) (Figures 6L–6O). These results suggested that Musk signaling stimulates AChR clustering by promoting Rapsn LLPS.

Decreased LLPS and cargo-carrying ability of CMS mutants

Numerous Rapsn mutations have been identified in individuals with CMS (Milone et al., 2009). Because a crystal structure of Rapsn is not available, we modeled Rapsn's structure based on the computer program I-TASSER (Roy et al., 2010). As shown in Figure 7A, the seven TPR motifs are grouped in the N-terminal region, followed by the CC domain and a seemingly loose RING domain. CMS mutations are distributed within the TPR region, the CC and RING domains, as well as in junction regions between these domains (Figure 7A). We wanted to find out whether CMS-associated mutations may alter Rapsn LLPS. Remarkably, the size of droplets formed by L14P, N88K, or R164H was smaller than that of Rapsn wild type (WT) at 5 μM (Figures 7B and 7C), suggesting a compromised ability for LLPS. Rapsn LLPS was not altered by 11 other CMS mutations, including those in the junction regions and in the CC and RING domains (Figures 7B and 7C; Table S1).

We determined the minimal concentrations of Rapsn WT and L14P, N88K, or R164H mutants for forming droplets and their sensitivity to increasing NaCl concentrations. Rapsn WT was able to phase-separate into droplets at 1 μM in the presence of 100 or 150 mM NaCl (Figure 7D), two concentrations close to physiological salt concentration. However, under these conditions, none of the three Rapsn mutants at 1 μM were able to form droplets (Figure 7D). The minimal concentrations for L14P, N88K, and R164H to form droplets increased to 3 μM and 5 μM, respectively, in the presence of 100 or 150 mM NaCl (Figure 7D). On the other hand, increasing NaCl concentrations inhibited LLPS of WT and mutant Rapsn (Figure 7D). However, Rapsn WT at 5 μM protein concentration was able to phase-separate into droplets at 300 mM NaCl, where LLPS was not observed for Rapsn mutants under the same conditions, even when the protein concentrations were increased to 8 μM (Figure 7D). Moreover, the puncta formed by L14P, N88K, or R164H were smaller than those formed by WT Rapsn in HEK293T cells (Figures 7E and 7F), indicating reduced LLPS in cells. It is worth noting that L14P, N88K, and R164H were localized in TPR motifs (TPR1, TPR3, and TPR5, respectively) (Figures 7G and 7H), consistent with the notion that multivalent binding of TPR motifs is critical for Rapsn LLPS (Figures 4 and S3). Intriguingly, the three mutations are located within the first α-helix (Figures 7G and 7H).

Of 14 CMS-associated mutations, 11 had no effect on Rapsn LLPS. We determined whether they alter the ability of Rapsn to recruit cargo proteins into condensates. As shown in Figures 7I and 7J, AChR-α and AChR-β were hardly detectable in droplets formed by L326P Rapsn, in contrast to a robust CF555 signal in droplets formed by WT Rapsn. These results indicate a critical role of L326 in carrying AChR-α and AChR-β into droplets. On the other hand, compared with WT Rapsn, E147K reduced the amount of MACF1 in the droplets, whereas 1177del2 inhibited recruitment of β-dystroglycan (Figures 7I and 7J). The effects of L326P, L147K, and 1177del2 on cargo-carrying ability was cargo specific, and they had no effect on co-condensation with other cargo proteins (Table S1). These results suggest two ways in which CMS-associated mutations impair NMJ formation: (1) preventing Rapsn from forming condensates and (2) impairing the ability of Rapsn to carry cargo proteins into condensates; this sheds light onto mechanisms of CMS pathology.

Diminished aneural and nerve-induced AChR clusters in R164H knockin mutant mice

We demonstrated that the N88K mutation prevented mice from forming proper NMJs (Xing et al., 2019), providing genetic evidence of a role of Rapsn LLPS in NMJ formation. To further test this hypothesis, we generated a knockin mouse strain carrying R164H (Figures S6A and S6B), a mutation in the fifth TRP motif that inhibits Rapsn LLPS (Figure 7). Self-association of R164H Rapsn was reduced compared with the WT (Figures S7A and S7B). The mutation had little effect on Rapsn mRNA and protein levels (Figures S6C and S6D) but prevented Rapsn from rescuing AChR clustering deficits in *Rapsn*$^{-/-}$ myotubes (Figures S7C and S7D). In WT mice, muscle fibers were dotted with primitive aneural AChR clusters in the central region on embryonic day 13.5 (E13.5) (a phenomenon called pre-patterning, prior to NMJ formation) (Li et al., 2018; Lin et al., 2001; Yang et al., 2000, 2001; Figure 8A). However, in R164H/R164H mice, aneural AChR clusters were barely detectable, a phenotype like that of Rapsn-null mice (*Rapsn*$^{-/-}$) (Figure 8A). Because R164H mice were generated by CRISPR-Cas9, we characterized R164H/− mice, in which one chromosome carried R164H and the other carried a null allele. Similar phenotypes were observed in R164H/− mice and R164H/R164H mice (Figure 8A), suggesting that NMJ deficits

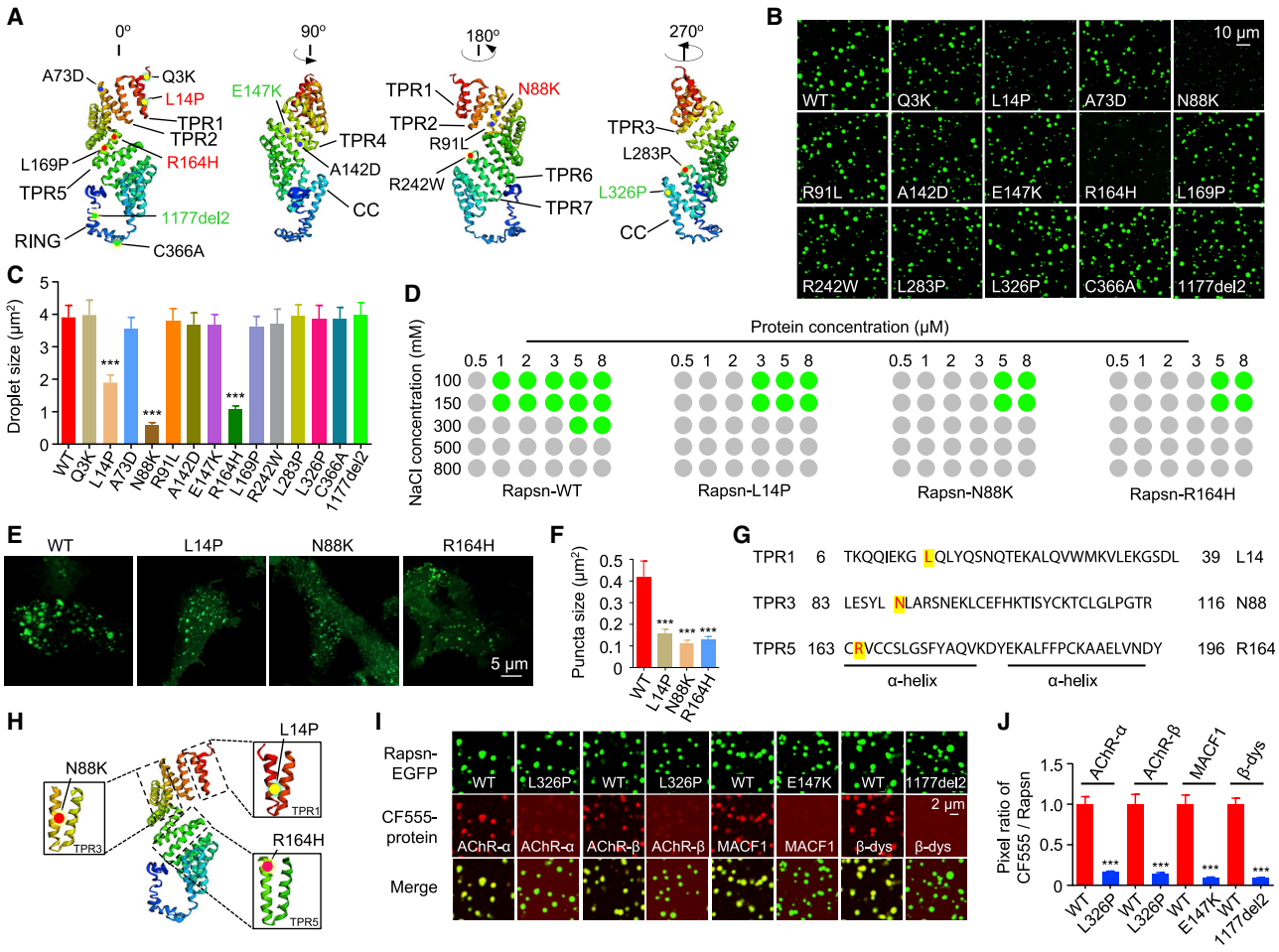

Figure 7. Decreased LLPS and cargo-carrying ability by CMS mutations

(A) Modeled structure of Rapsn and localization of CMS mutations. Red, mutations that reduce Rapsn LLPS; green, mutations that decrease cargo recruitment.

(B) Representative images showing condensed droplets formed by LLPS of WT or the indicated mutant Rapsn (5 μM).

(C) Quantification of droplet size in (B). n = 3, ***p < 0.001, one-way ANOVA.

(D) Phase diagrams showing droplet formation of WT or three mutant Rapsn (L14P, N88K, and R164H) with different protein concentrations in 25 mM Tris (pH 7.4), 5 mM DTT, and NaCl (ranging from 100–800 mM). Green dots, phase separation; gray dots, no phase separation.

(E) Mutant Rapsn (L14P, N88K, and R164H) forms smaller puncta compared with WT Rapsn in transfected HEK293T cells.

(F) Quantification of punctum size in (E). n = 10, ***p < 0.001, one-way ANOVA.

(G and H) Location of LLPS-inhibiting mutations in the first α helix.

(I) Recruitment of cargo proteins into Rapsn condensates was inhibited by CMS-related mutations.

(J) Quantification of the pixel ratio of CF555/Rapsn-EGFP in (I). n = 3, ***p < 0.001, one-way ANOVA.

Data are shown as mean ± SEM. See also Table S1.

were not an off-target effect. These results suggest that the R164H mutation impaired formation of aneural AChR clusters.

In WT mice, innervation occurs on ~E14.5, induces larger clusters, and disperses aneural clusters. As shown in Figures 8A, 8C, and 8D, the numbers and sizes of AChR clusters were reduced in R164H/R164H and R164H/− mice at age of E16 compared with WT controls. At P0, AChR clusters appear as oval plaques that are distributed within a restricted central region in WT mice (Figure 8B). However, in R164H/R164H and R164H/− mice, AChR clusters were smaller in size with reduced intensity and distributed in a wider center area (Figures 8B, 8C, and 8E), indicating that R164 is necessary for nerve-induced AChR clustering. R164H had little effect on Rapsn stability or interaction with AChR, actin, or other binding partners, including β-dystroglycan, calpain, MACF1, and α-actinin (Figures S7E–S7M). These results provide further genetic evidence of a role of Rapsn LLPS in NMJ formation. In addition to postsynaptic deficits, motor nerve terminals arborized extensively in R164H mutant mice (Figures 8B, 8D, 8F, and 8G), a phenotype commonly observed in mice with mutant Rapsn, LRP4, Musk, or Dok7 (DeChiara et al., 1996; Gautam et al., 1995; Okada et al., 2006; Weatherbee et al., 2006). The cause of presynaptic deficits is unclear but may be due to a compensatory mechanism for postsynaptic deficits and/or loss of retrograde

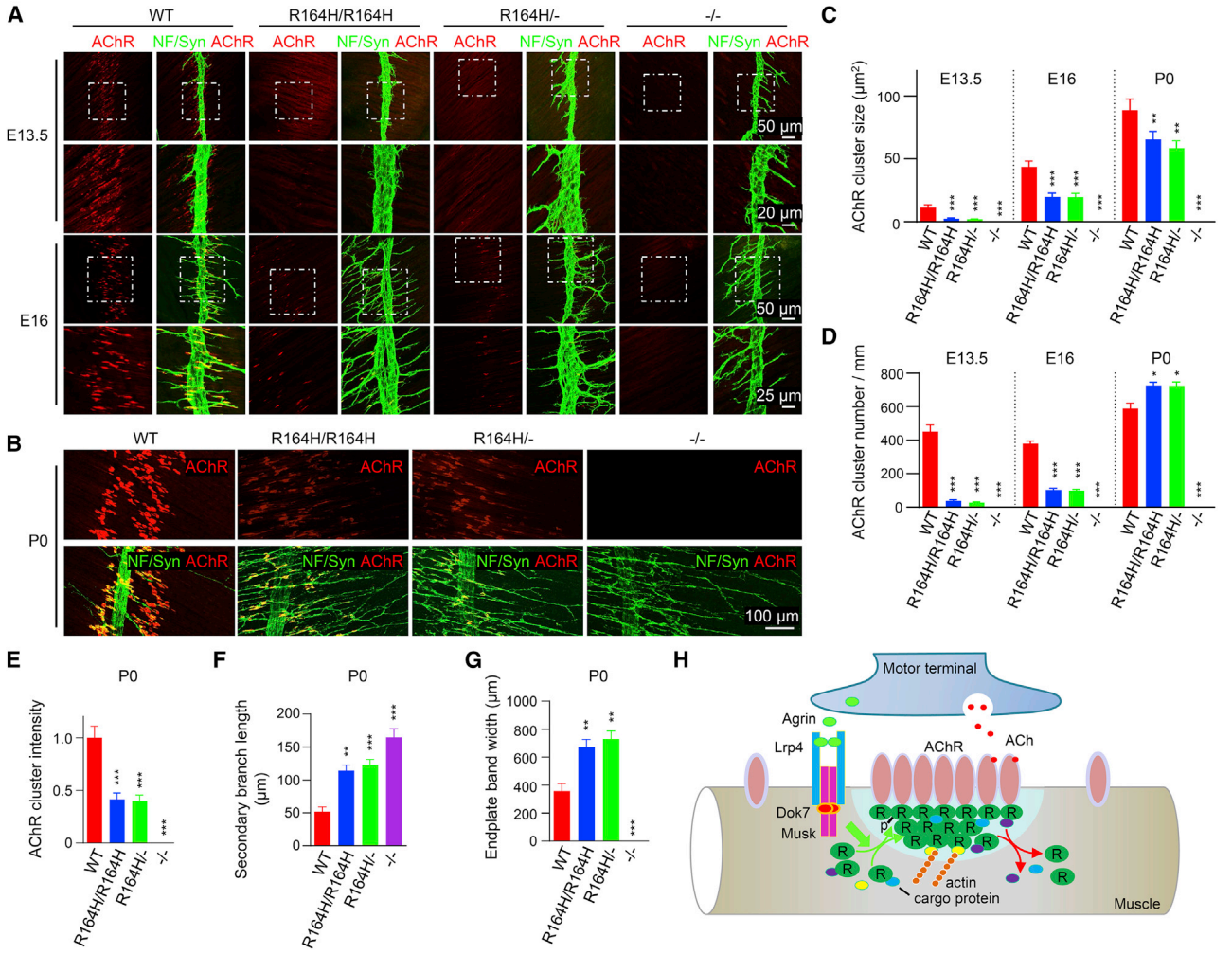

Figure 8. Diminished aneural and nerve-induced AChR clusters in R164H knockin mutant mice

(A and B) Diminished aneural and nerve-induced AChR clusters in R164H knockin mutant mice. Diaphragms of the indicated genotypes at different ages were stained whole mount with Fluor 594-α-BTX (Bungarotoxin, red) to label AChR clusters and with anti-NF/Syn (Neurofilament/Synapsin, green) antibodies to label motor nerve terminals. Areas in rectangles in the top panels are shown magnified in the bottom panels (A).

(C–G) Quantitative data showing AChR cluster size (C) and number (D), AChR intensity (E), secondary nerve branch length (F), and endplate band width (G). Data are shown as mean ± SEM; n = 3, *p < 0.05, **p < 0.01, ***p < 0.001, one-way ANOVA.

(H) Working model. Rapsn condensates to form a liquid-like semi-membraneless compartment. In so doing, Rapsn recruits cargo proteins that regulate AChR clustering. These condensates may serve as a hub that promotes cytoskeletal interaction and are promoted by agrin-LRP4-Musk signaling.

See also Figures S6 and S7.

signaling directly or indirectly downstream of the agrin pathway (DeChiara et al., 1996).

DISCUSSION

We provide evidence that Rapsn undergoes LLPS into dynamic condensates *in vitro*, in HEK293T cells, and in muscle (Figures 1, 2, and 3). Rapsn condensates can co-condensate AChRs as well as cytoskeletal and signaling proteins (Figures 5B and 5C). Remarkably, the capacity of Rapsn to phase-separate and co-condensate with cargo proteins is compromised by CMS-associated mutations (Figure 7). In particular, N88K, a prevalent CMS-related mutation in Rapsn, reduced LLPS of Rapsn; NMJ formation is impaired in N88K mutant mice (Xing et al., 2019). Here we show that R164H, another CMS mutation, inhibits Rapsn LLPS and prevents proper NMJ assembly (Figures 7 and 8), providing genetic evidence of Rapsn LLPS in NMJ formation and revealing potential pathological mechanisms of neuromuscular disorders.

Our results support a working model where Rapsn condensates to form a membraneless subcellular compartment to orchestrate NMJ assembly (Figure 8H) in two ways. First, Rapsn compartments co-condensate with AChR subunits and cytoskeletal proteins directly or indirectly (Figure 5B), suggesting that Rapsn LLPS serves as a structural platform for AChR clustering and anchoring AChRs to the cytoskeleton. Because its

ability to condensate without an extrinsic regulator, Rapsn is sufficient to initiate AChR clustering in muscle prior to innervation by motor neurons. Interestingly, Rapsn is more conserved than many NMJ proteins across the species; for example, *C. elegans* expresses Rapsn but not agrin, LRP4, or Musk. Therefore, Rapsn may play a key role in synaptogenesis in species before complex regulatory mechanisms evolve. Second, Rapsn condensates may function as a signaling hub to favor AChR clustering. LLPS was more robust by Rapsn purified from cells that expressed WT, but not Musk-KD (Figures 6G–6J), suggesting that Rapsn LLPS could be promoted by agrin-LRP4-Musk signaling. In addition, signaling molecules, including protein kinase A (PKA) (Choi et al., 2012), CK2 (Herrmann et al., 2015), and HSP90β (Luo et al., 2008), could be recruited to the condensates through direct or indirect binding. Bringing together Rapsn (an E3 ligase) and AChR subunits, Rapsn LLPS may facilitate AChR neddylation, which is required for AChR stability (Li et al., 2016; Xing et al., 2020). Consistent with this notion, N88K mutation, which reduces LLPS of Rapsn, also reduces AChR neddylation (Xing et al., 2019).

Rapsn is a major target of CMS, accounting for 15% of total CMS cases (Milone et al., 2009). Rapsn mutations can reduce Rapsn's ability to induce AChR clustering (Cossins et al., 2006; Maselli et al., 2003, 2007; Ohno et al., 2002, 2003). However, little is known regarding the underlying molecular mechanisms. Here, we demonstrate that L14P, N88K, and R164H diminish the ability of Rapsn to condensate in solution and in cells (Figure 7). On the other hand, three other mutations, L326P, E147K, and 1177del2, have no effect on Rapsn LLPS but prevent Rapsn from carrying interacting proteins into condensates (Figure 7). These results reveal a novel pathological mechanism of CMS mutations; i.e., by disrupting formation of a semi-membraneless compartment or recruitment of signaling proteins into the compartment. Some CMS mutations had no effect on Rapsn LLPS or co-condensation. This may reflect failure to interact with other cargos that were not tested or another mechanism that is distinct from altering LLPS or cargo interactions.

Unlike the PSD of brain synapses, the NMJ does not have a postsynaptic electron density structure. LLPS by PSD proteins requires interactions of two or three organizers. For example, PSD-95, SynGAP, Shank, GKAP, and Homer do not condensate individually; however, PSD-95 and SynGAP or Shank, Homer and GAKP, when mixed, can phase-separate (Zeng et al., 2016, 2018). The resulting condensates can recruit other PSD-associated proteins and cluster glutamatergic receptors (Zeng et al., 2018). Evidently, Rapsn alone is able to phase-separate to form droplets through multivalent binding of the TPR domain. A TPR motif is composed of 34 amino acids that could mediate oligomerization of TPR-containing proteins (Blatch and Lässle, 1999; Zeytuni and Zarivach, 2012). Indeed, Rapsn self-associates through TPRs (Ramarao et al., 2001; Xing et al., 2019). We show that two or more of the TPRs, except TPR6–7, can interact with one another or self-associate; such multivalent binding is critical for Rapsn LLPS. TPR domains exist in many proteins critical for neural development, including FKBP52, important for neuronal differentiation (Quintá and Galigniana, 2012); postsynaptic scaffold proteins of the TANC (tetratricopeptide repeat, ankyrin repeat and coiled-coil containing) family that bind PSD95 (Han et al., 2010); and TRIP8b, an adaptor protein for channel trafficking (Lewis et al., 2011). Our results suggest that LLPS may be involved in many aspects of neuronal function.

STAR★METHODS

Detailed methods are provided in the online version of this paper and include the following:

- KEY RESOURCES TABLE
- RESOURCE AVAILABILITY
  - Lead contact
  - Materials availability
  - Data and code availability
- EXPERIMENTAL MODEL AND SUBJECT DETAILS
  - Mice
- METHOD DETAILS
  - Protein expression, purification, and fluorescence labeling
  - Phase separation of proteins *in vitro* and imaging
  - Co-immunoprecipitation assay
  - FRAP assay
  - Immunofluorescence staining
  - Live cell imaging and quantification of Rapsn-EGFP concentration in cells
  - Isolation of phase-separated condensates from aqueous phase
  - Silver staining
  - CK2 and Src kinase assay
  - Real time PCR
- QUANTIFICATION AND STATISTICAL ANALYSIS

SUPPLEMENTAL INFORMATION

Supplemental information can be found online at https://doi.org/10.1016/j.neuron.2021.04.021.

ACKNOWLEDGMENTS

We thank Dr. Rajendra Boggavarapu for helping with purification of proteins and members of the Mei/Xiong Lab for discussions. This study was supported by grants from Veterans Affairs and the NIH (to L.M. and W.C.X.).

AUTHOR CONTRIBUTIONS

L.M., W.-C.X., and G.X. conceived the study. G.X., H.J., Z.Y., P.C., and H.W. performed the experiments. G.X., H.J., and Z.Y. analyzed the data. L.M. and G.X. wrote the manuscript.

DECLARATION OF INTERESTS

The authors declare no competing interests.

Received: January 5, 2021
Revised: March 27, 2021
Accepted: April 22, 2021
Published: May 24, 2021

REFERENCES

Alberti, S., and Dormann, D. (2019). Liquid-Liquid Phase Separation in Disease. Annu. Rev. Genet. *53*, 171–194.

Antolik, C., Catino, D.H., O'Neill, A.M., Resneck, W.G., Ursitti, J.A., and Bloch, R.J. (2007). The actin binding domain of ACF7 binds directly to the tetratricopeptide repeat domains of rapsyn. Neuroscience *145*, 56–65.

Bai, G., Wang, Y., and Zhang, M. (2021). Gephyrin-mediated formation of inhibitory postsynaptic density sheet via phase separation. Cell Res. *31*, 312–325.

Bartoli, M., Ramarao, M.K., and Cohen, J.B. (2001). Interactions of the rapsyn RING-H2 domain with dystroglycan. J. Biol. Chem. *276*, 24911–24917.

Beutel, O., Maraspini, R., Pombo-García, K., Martin-Lemaitre, C., and Honigmann, A. (2019). Phase Separation of Zonula Occludens Proteins Drives Formation of Tight Junctions. Cell *179*, 923–936.e11.

Blatch, G.L., and Lässle, M. (1999). The tetratricopeptide repeat: a structural motif mediating protein-protein interactions. BioEssays *21*, 932–939.

Boeynaems, S., Alberti, S., Fawzi, N.L., Mittag, T., Polymenidou, M., Rousseau, F., Schymkowitz, J., Shorter, J., Wolozin, B., Van Den Bosch, L., et al. (2018). Protein Phase Separation: A New Phase in Cell Biology. Trends Cell Biol. *28*, 420–435.

Boija, A., Klein, I.A., Sabari, B.R., Dall'Agnese, A., Coffey, E.L., Zamudio, A.V., Li, C.H., Shrinivas, K., Manteiga, J.C., Hannett, N.M., et al. (2018). Transcription Factors Activate Genes through the Phase-Separation Capacity of Their Activation Domains. Cell *175*, 1842–1855.e16.

Cappello, V., and Francolini, M. (2017). Neuromuscular Junction Dismantling in Amyotrophic Lateral Sclerosis. Int. J. Mol. Sci. *18*, 2092.

Chen, F., Qian, L., Yang, Z.H., Huang, Y., Ngo, S.T., Ruan, N.J., Wang, J., Schneider, C., Noakes, P.G., Ding, Y.Q., et al. (2007). Rapsyn interaction with calpain stabilizes AChR clusters at the neuromuscular junction. Neuron *55*, 247–260.

Chen, X., Wu, X., Wu, H., and Zhang, M. (2020). Phase separation at the synapse. Nat. Neurosci. *23*, 301–310.

Cheusova, T., Khan, M.A., Schubert, S.W., Gavin, A.C., Buchou, T., Jacob, G., Sticht, H., Allende, J., Boldyreff, B., Brenner, H.R., and Hashemolhosseini, S. (2006). Casein kinase 2-dependent serine phosphorylation of MuSK regulates acetylcholine receptor aggregation at the neuromuscular junction. Genes Dev. *20*, 1800–1816.

Choi, K.R., Berrera, M., Reischl, M., Strack, S., Albrizio, M., Röder, I.V., Wagner, A., Petersen, Y., Hafner, M., Zaccolo, M., and Rudolf, R. (2012). Rapsyn mediates subsynaptic anchoring of PKA type I and stabilisation of acetylcholine receptor in vivo. J. Cell Sci. *125*, 714–723.

Cossins, J., Burke, G., Maxwell, S., Spearman, H., Man, S., Kuks, J., Vincent, A., Palace, J., Fuhrer, C., and Beeson, D. (2006). Diverse molecular mechanisms involved in AChR deficiency due to rapsyn mutations. Brain *129*, 2773–2783.

DeChiara, T.M., Bowen, D.C., Valenzuela, D.M., Simmons, M.V., Poueymirou, W.T., Thomas, S., Kinetz, E., Compton, D.L., Rojas, E., Park, J.S., et al. (1996). The receptor tyrosine kinase MuSK is required for neuromuscular junction formation in vivo. Cell *85*, 501–512.

Dobbins, G.C., Luo, S., Yang, Z., Xiong, W.C., and Mei, L. (2008). alpha-Actinin interacts with rapsyn in agrin-stimulated AChR clustering. Mol. Brain *1*, 18.

Eiber, N., Rehman, M., Kravic, B., Rudolf, R., Sandri, M., and Hashemolhosseini, S. (2019). Loss of Protein Kinase Csnk2b/CK2β at Neuromuscular Junctions Affects Morphology and Dynamics of Aggregated Nicotinic Acetylcholine Receptors, Neuromuscular Transmission, and Synaptic Gene Expression. Cells *8*, 940.

Engel, A.G., Shen, X.M., Selcen, D., and Sine, S.M. (2015). Congenital myasthenic syndromes: pathogenesis, diagnosis, and treatment. Lancet Neurol. *14*, 420–434.

Fambrough, D.M., Drachman, D.B., and Satyamurti, S. (1973). Neuromuscular junction in myasthenia gravis: decreased acetylcholine receptors. Science *182*, 293–295.

Feng, Z., Chen, X., Zeng, M., and Zhang, M. (2019). Phase separation as a mechanism for assembling dynamic postsynaptic density signalling complexes. Curr. Opin. Neurobiol. *57*, 1–8.

Fertuck, H.C., and Salpeter, M.M. (1976). Quantitation of junctional and extrajunctional acetylcholine receptors by electron microscope autoradiography after 125I-alpha-bungarotoxin binding at mouse neuromuscular junctions. J. Cell Biol. *69*, 144–158.

Flanagan-Steet, H., Fox, M.A., Meyer, D., and Sanes, J.R. (2005). Neuromuscular synapses can form in vivo by incorporation of initially aneural postsynaptic specializations. Development *132*, 4471–4481.

Frail, D.E., McLaughlin, L.L., Mudd, J., and Merlie, J.P. (1988). Identification of the mouse muscle 43,000-dalton acetylcholine receptor-associated protein (RAPsyn) by cDNA cloning. J. Biol. Chem. *263*, 15602–15607.

Froehner, S.C., Luetje, C.W., Scotland, P.B., and Patrick, J. (1990). The postsynaptic 43K protein clusters muscle nicotinic acetylcholine receptors in Xenopus oocytes. Neuron *5*, 403–410.

Fuhrer, C., Gautam, M., Sugiyama, J.E., and Hall, Z.W. (1999). Roles of rapsyn and agrin in interaction of postsynaptic proteins with acetylcholine receptors. J. Neurosci. *19*, 6405–6416.

Gautam, M., Noakes, P.G., Mudd, J., Nichol, M., Chu, G.C., Sanes, J.R., and Merlie, J.P. (1995). Failure of postsynaptic specialization to develop at neuromuscular junctions of rapsyn-deficient mice. Nature *377*, 232–236.

Gilhus, N.E., Tzartos, S., Evoli, A., Palace, J., Burns, T.M., and Verschuuren, J.J.G.M. (2019). Myasthenia gravis. Nat. Rev. Dis. Primers *5*, 30.

Glass, D.J., Bowen, D.C., Stitt, T.N., Radziejewski, C., Bruno, J., Ryan, T.E., Gies, D.R., Shah, S., Mattsson, K., Burden, S.J., et al. (1996). Agrin acts via a MuSK receptor complex. Cell *85*, 513–523.

Guo, C., Che, Z., Yue, J., Xie, P., Hao, S., Xie, W., Luo, Z., and Lin, C. (2020). ENL initiates multivalent phase separation of the super elongation complex (SEC) in controlling rapid transcriptional activation. Sci. Adv. *6*, eaay4858.

Han, H., Noakes, P.G., and Phillips, W.D. (1999). Overexpression of rapsyn inhibits agrin-induced acetylcholine receptor clustering in muscle cells. J. Neurocytol. *28*, 763–775.

Han, S., Nam, J., Li, Y., Kim, S., Cho, S.H., Cho, Y.S., Choi, S.Y., Choi, J., Han, K., Kim, Y., et al. (2010). Regulation of dendritic spines, spatial memory, and embryonic development by the TANC family of PSD-95-interacting proteins. J. Neurosci. *30*, 15102–15112.

Hernández-Vega, A., Braun, M., Scharrel, L., Jahnel, M., Wegmann, S., Hyman, B.T., Alberti, S., Diez, S., and Hyman, A.A. (2017). Local Nucleation of Microtubule Bundles through Tubulin Concentration into a Condensed Tau Phase. Cell Rep. *20*, 2304–2312.

Herrmann, D., Straubinger, M., and Hashemolhosseini, S. (2015). Protein kinase CK2 interacts at the neuromuscular synapse with Rapsyn, Rac1, 14-3-3γ, and Dok-7 proteins and phosphorylates the latter two. J. Biol. Chem. *290*, 22370–22384.

Hofweber, M., Hutten, S., Bourgeois, B., Spreitzer, E., Niedner-Boblenz, A., Schifferer, M., Ruepp, M.D., Simons, M., Niessing, D., Madl, T., and Dormann, D. (2018). Phase Separation of FUS Is Suppressed by Its Nuclear Import Receptor and Arginine Methylation. Cell *173*, 706–719.e13.

Jennings, C.G., Dyer, S.M., and Burden, S.J. (1993). Muscle-specific trk-related receptor with a kringle domain defines a distinct class of receptor tyrosine kinases. Proc. Natl. Acad. Sci. USA *90*, 2895–2899.

Kim, N., Stiegler, A.L., Cameron, T.O., Hallock, P.T., Gomez, A.M., Huang, J.H., Hubbard, S.R., Dustin, M.L., and Burden, S.J. (2008). Lrp4 is a receptor for Agrin and forms a complex with MuSK. Cell *135*, 334–342.

Lee, Y., Rudell, J., Yechikhov, S., Taylor, R., Swope, S., and Ferns, M. (2008). Rapsyn carboxyl terminal domains mediate muscle specific kinase-induced phosphorylation of the muscle acetylcholine receptor. Neuroscience *153*, 997–1007.

Lee, Y., Rudell, J., and Ferns, M. (2009). Rapsyn interacts with the muscle acetylcholine receptor via alpha-helical domains in the alpha, beta, and epsilon subunit intracellular loops. Neuroscience *163*, 222–232.

Lewis, A.S., Vaidya, S.P., Blaiss, C.A., Liu, Z., Stoub, T.R., Brager, D.H., Chen, X., Bender, R.A., Estep, C.M., Popov, A.B., et al. (2011). Deletion of the hyperpolarization-activated cyclic nucleotide-gated channel auxiliary subunit

TRIP8b impairs hippocampal Ih localization and function and promotes antidepressant behavior in mice. J. Neurosci. *31*, 7424–7440.

Li, L., Cao, Y., Wu, H., Ye, X., Zhu, Z., Xing, G., Shen, C., Barik, A., Zhang, B., Xie, X., et al. (2016). Enzymatic Activity of the Scaffold Protein Rapsyn for Synapse Formation. Neuron *92*, 1007–1019.

Li, L., Xiong, W.C., and Mei, L. (2018). Neuromuscular Junction Formation, Aging, and Disorders. Annu. Rev. Physiol. *80*, 159–188.

Lin, W., Burgess, R.W., Dominguez, B., Pfaff, S.L., Sanes, J.R., and Lee, K.F. (2001). Distinct roles of nerve and muscle in postsynaptic differentiation of the neuromuscular synapse. Nature *410*, 1057–1064.

Lin, W., Dominguez, B., Yang, J., Aryal, P., Brandon, E.P., Gage, F.H., and Lee, K.F. (2005). Neurotransmitter acetylcholine negatively regulates neuromuscular synapse formation by a Cdk5-dependent mechanism. Neuron *46*, 569–579.

Liu, Y., Padgett, D., Takahashi, M., Li, H., Sayeed, A., Teichert, R.W., Olivera, B.M., McArdle, J.J., Green, W.N., and Lin, W. (2008). Essential roles of the acetylcholine receptor gamma-subunit in neuromuscular synaptic patterning. Development *135*, 1957–1967.

Luo, S., Zhang, B., Dong, X.P., Tao, Y., Ting, A., Zhou, Z., Meixiong, J., Luo, J., Chiu, F.C., Xiong, W.C., and Mei, L. (2008). HSP90 beta regulates rapsyn turnover and subsequent AChR cluster formation and maintenance. Neuron *60*, 97–110.

Maselli, R.A., Dunne, V., Pascual-Pascual, S.I., Bowe, C., Agius, M., Frank, R., and Wollmann, R.L. (2003). Rapsyn mutations in myasthenic syndrome due to impaired receptor clustering. Muscle Nerve *28*, 293–301.

Maselli, R., Dris, H., Schnier, J., Cockrell, J., and Wollmann, R. (2007). Congenital myasthenic syndrome caused by two non-N88K rapsyn mutations. Clin. Genet. *72*, 63–65.

McDonald, N.A., Fetter, R.D., and Shen, K. (2020). Assembly of synaptic active zones requires phase separation of scaffold molecules. Nature *588*, 454–458.

McMahan, U.J. (1990). The agrin hypothesis. Cold Spring Harb. Symp. Quant. Biol. *55*, 407–418.

Milone, M., Shen, X.M., Selcen, D., Ohno, K., Brengman, J., Iannaccone, S.T., Harper, C.M., and Engel, A.G. (2009). Myasthenic syndrome due to defects in rapsyn: Clinical and molecular findings in 39 patients. Neurology *73*, 228–235.

Milovanovic, D., Wu, Y., Bian, X., and De Camilli, P. (2018). A liquid phase of synapsin and lipid vesicles. Science *361*, 604–607.

Misgeld, T., Kummer, T.T., Lichtman, J.W., and Sanes, J.R. (2005). Agrin promotes synaptic differentiation by counteracting an inhibitory effect of neurotransmitter. Proc. Natl. Acad. Sci. USA *102*, 11088–11093.

Molliex, A., Temirov, J., Lee, J., Coughlin, M., Kanagaraj, A.P., Kim, H.J., Mittag, T., and Taylor, J.P. (2015). Phase separation by low complexity domains promotes stress granule assembly and drives pathological fibrillization. Cell *163*, 123–133.

Murakami, T., Qamar, S., Lin, J.Q., Schierle, G.S., Rees, E., Miyashita, A., Costa, A.R., Dodd, R.B., Chan, F.T., Michel, C.H., et al. (2015). ALS/FTD Mutation-Induced Phase Transition of FUS Liquid Droplets and Reversible Hydrogels into Irreversible Hydrogels Impairs RNP Granule Function. Neuron *88*, 678–690.

Neubig, R.R., and Cohen, J.B. (1979). Equilibrium binding of [3H]tubocurarine and [3H]acetylcholine by Torpedo postsynaptic membranes: stoichiometry and ligand interactions. Biochemistry *18*, 5464–5475.

Ohno, K., Engel, A.G., Shen, X.M., Selcen, D., Brengman, J., Harper, C.M., Tsujino, A., and Milone, M. (2002). Rapsyn mutations in humans cause endplate acetylcholine-receptor deficiency and myasthenic syndrome. Am. J. Hum. Genet. *70*, 875–885.

Ohno, K., Sadeh, M., Blatt, I., Brengman, J.M., and Engel, A.G. (2003). E-box mutations in the RAPSN promoter region in eight cases with congenital myasthenic syndrome. Hum. Mol. Genet. *12*, 739–748.

Okada, K., Inoue, A., Okada, M., Murata, Y., Kakuta, S., Jigami, T., Kubo, S., Shiraishi, H., Eguchi, K., Motomura, M., et al. (2006). The muscle protein Dok-7 is essential for neuromuscular synaptogenesis. Science *312*, 1802–1805.

Oury, J., Liu, Y., Töpf, A., Todorovic, S., Hoedt, E., Preethish-Kumar, V., Neubert, T.A., Lin, W., Lochmüller, H., and Burden, S.J. (2019). MACF1 links Rapsyn to microtubule- and actin-binding proteins to maintain neuromuscular synapses. J. Cell Biol. *218*, 1686–1705.

Perez-Riba, A., and Itzhaki, L.S. (2019). The tetratricopeptide-repeat motif is a versatile platform that enables diverse modes of molecular recognition. Curr. Opin. Struct. Biol. *54*, 43–49.

Phillips, W.D., Kopta, C., Blount, P., Gardner, P.D., Steinbach, J.H., and Merlie, J.P. (1991). ACh receptor-rich membrane domains organized in fibroblasts by recombinant 43-kildalton protein. Science *251*, 568–570.

Quintá, H.R., and Galigniana, M.D. (2012). The neuroregenerative mechanism mediated by the Hsp90-binding immunophilin FKBP52 resembles the early steps of neuronal differentiation. Br. J. Pharmacol. *166*, 637–649.

Ramarao, M.K., Bianchetta, M.J., Lanken, J., and Cohen, J.B. (2001). Role of rapsyn tetratricopeptide repeat and coiled-coil domains in self-association and nicotinic acetylcholine receptor clustering. J. Biol. Chem. *276*, 7475–7483.

Rio, D.C., Ares, M., Jr., Hannon, G.J., and Nilsen, T.W. (2010). Purification of RNA using TRIzol (TRI reagent). Cold Spring Harb. Protoc. *2010*, pdb.prot5439.

Roy, A., Kucukural, A., and Zhang, Y. (2010). I-TASSER: a unified platform for automated protein structure and function prediction. Nat. Protoc. *5*, 725–738.

Sanes, J.R., and Lichtman, J.W. (1999). Development of the vertebrate neuromuscular junction. Annu. Rev. Neurosci. *22*, 389–442.

Schwayer, C., Shamipour, S., Pranjic-Ferscha, K., Schauer, A., Balda, M., Tada, M., Matter, K., and Heisenberg, C.P. (2019). Mechanosensation of Tight Junctions Depends on ZO-1 Phase Separation and Flow. Cell *179*, 937–952.e18.

Shevchenko, A., Wilm, M., Vorm, O., and Mann, M. (1996). Mass spectrometric sequencing of proteins silver-stained polyacrylamide gels. Anal. Chem. *68*, 850–858.

Shi, L., Fu, A.K., and Ip, N.Y. (2012). Molecular mechanisms underlying maturation and maintenance of the vertebrate neuromuscular junction. Trends Neurosci. *35*, 441–453.

Shin, Y., and Brangwynne, C.P. (2017). Liquid phase condensation in cell physiology and disease. Science *357*, eaaf4382.

Sjöblom, B., Salmazo, A., and Djinović-Carugo, K. (2008). Alpha-actinin structure and regulation. Cell. Mol. Life Sci. *65*, 2688–2701.

Sobel, A., Heidmann, T., Hofler, J., and Changeux, J.P. (1978). Distinct protein components from Torpedo marmorata membranes carry the acetylcholine receptor site and the binding site for local anesthetics and histrionicotoxin. Proc. Natl. Acad. Sci. USA *75*, 510–514.

Tintignac, L.A., Brenner, H.R., and Rüegg, M.A. (2015). Mechanisms Regulating Neuromuscular Junction Development and Function and Causes of Muscle Wasting. Physiol. Rev. *95*, 809–852.

Walker, J.H., Boustead, C.M., and Witzemann, V. (1984). The 43-K protein, v1, associated with acetylcholine receptor containing membrane fragments is an actin-binding protein. EMBO J. *3*, 2287–2290.

Weatherbee, S.D., Anderson, K.V., and Niswander, L.A. (2006). LDL-receptor-related protein 4 is crucial for formation of the neuromuscular junction. Development *133*, 4993–5000.

Wilfling, F., Lee, C.W., Erdmann, P.S., Zheng, Y., Sherpa, D., Jentsch, S., Pfander, B., Schulman, B.A., and Baumeister, W. (2020). A Selective Autophagy Pathway for Phase-Separated Endocytic Protein Deposits. Mol. Cell *80*, 764–778.e7.

Woodruff, J.B., Ferreira Gomes, B., Widlund, P.O., Mahamid, J., Honigmann, A., and Hyman, A.A. (2017). The Centrosome Is a Selective Condensate that Nucleates Microtubules by Concentrating Tubulin. Cell *169*, 1066–1077.e10.

Wu, H., Xiong, W.C., and Mei, L. (2010). To build a synapse: signaling pathways in neuromuscular junction assembly. Development *137*, 1017–1033.

Wu, X., Cai, Q., Shen, Z., Chen, X., Zeng, M., Du, S., and Zhang, M. (2019). RIM and RIM-BP Form Presynaptic Active-Zone-like Condensates via Phase Separation. Mol. Cell *73*, 971–984.e5.

Wu, X., Cai, Q., Feng, Z., and Zhang, M. (2020). Liquid-Liquid Phase Separation in Neuronal Development and Synaptic Signaling. Dev. Cell *55*, 18–29.

Xing, G., Jing, H., Zhang, L., Cao, Y., Li, L., Zhao, K., Dong, Z., Chen, W., Wang, H., Cao, R., et al. (2019). A mechanism in agrin signaling revealed by a prevalent Rapsyn mutation in congenital myasthenic syndrome. eLife *8*, e49180.

Xing, G., Xiong, W.C., and Mei, L. (2020). Rapsyn as a signaling and scaffolding molecule in neuromuscular junction formation and maintenance. Neurosci. Lett. *731*, 135013.

Yang, X., Li, W., Prescott, E.D., Burden, S.J., and Wang, J.C. (2000). DNA topoisomerase IIbeta and neural development. Science *287*, 131–134.

Yang, X., Arber, S., William, C., Li, L., Tanabe, Y., Jessell, T.M., Birchmeier, C., and Burden, S.J. (2001). Patterning of muscle acetylcholine receptor gene expression in the absence of motor innervation. Neuron *30*, 399–410.

Yoshihara, C.M., and Hall, Z.W. (1993). Increased expression of the 43-kD protein disrupts acetylcholine receptor clustering in myotubes. J. Cell Biol. *122*, 169–179.

Zeng, M., Shang, Y., Araki, Y., Guo, T., Huganir, R.L., and Zhang, M. (2016). Phase Transition in Postsynaptic Densities Underlies Formation of Synaptic Complexes and Synaptic Plasticity. Cell *166*, 1163–1175.e12.

Zeng, M., Chen, X., Guan, D., Xu, J., Wu, H., Tong, P., and Zhang, M. (2018). Reconstituted Postsynaptic Density as a Molecular Platform for Understanding Synapse Formation and Plasticity. Cell *174*, 1172–1187.e16.

Zeng, M., Díaz-Alonso, J., Ye, F., Chen, X., Xu, J., Ji, Z., Nicoll, R.A., and Zhang, M. (2019). Phase Separation-Mediated TARP/MAGUK Complex Condensation and AMPA Receptor Synaptic Transmission. Neuron *104*, 529–543.e6.

Zeytuni, N., and Zarivach, R. (2012). Structural and functional discussion of the tetra-trico-peptide repeat, a protein interaction module. Structure *20*, 397–405.

Zhang, B., Luo, S., Wang, Q., Suzuki, T., Xiong, W.C., and Mei, L. (2008). LRP4 serves as a coreceptor of agrin. Neuron *60*, 285–297.

Zhang, B., Liang, C., Bates, R., Yin, Y., Xiong, W.C., and Mei, L. (2012). Wnt proteins regulate acetylcholine receptor clustering in muscle cells. Mol. Brain *5*, 7.

Zhang, G., Wang, Z., Du, Z., and Zhang, H. (2018). mTOR Regulates Phase Separation of PGL Granules to Modulate Their Autophagic Degradation. Cell *174*, 1492–1506.e22.

Zhang, H., Sathyamurthy, A., Liu, F., Li, L., Zhang, L., Dong, Z., Cui, W., Sun, X., Zhao, K., Wang, H., et al. (2019). Agrin-Lrp4-Ror2 signaling regulates adult hippocampal neurogenesis in mice. eLife *8*, e45303.

Zhao, K., Shen, C., Li, L., Wu, H., Xing, G., Dong, Z., Jing, H., Chen, W., Zhang, H., Tan, Z., et al. (2018). Sarcoglycan Alpha Mitigates Neuromuscular Junction Decline in Aged Mice by Stabilizing LRP4. J. Neurosci. *38*, 8860–8873.

Zhu, G., Xie, J., Kong, W., Xie, J., Li, Y., Du, L., Zheng, Q., Sun, L., Guan, M., Li, H., et al. (2020). Phase Separation of Disease-Associated SHP2 Mutants Underlies MAPK Hyperactivation. Cell *183*, 490–502.e18.

STAR★METHODS

KEY RESOURCES TABLE

REAGENT or RESOURCE	SOURCE	IDENTIFIER
Antibodies		
Anti-GFP	Cell signaling technology	Cat#: 2555; RRID: AB_10692764
Anti-p-Tyr-100	Cell signaling technology	Cat #: 9411; RRID: AB_331228
Anti-p-Thr/Ser	Cell signaling technology	Cat #: 9631; RRID: AB_330308
Anti-Actin	Cell signaling technology	Cat #: 4967; RRID: AB_330288
Anti-synapsin-1	Cell signaling technology	Cat #: 5297; RRID: AB_2616578
Anti-neurofilament	Cell signaling technology	Cat #: 2837S; RRID: AB_823575
Anti-Flag	Sigma	Cat #: F7425;
Anti-HA	Sigma	Cat#: H6908; RRID: AB_260070
Anti-Myc	Sigma	Cat#: C3956; RRID: AB_439680
Mouse anti-Flag M2 affinity gel	Sigma	Cat #: A2220; RRID: AB_10063035
Anti-GAPDH	Santa Cruz	Cat #: sc-32233; RRID: AB_627679
Mouse monoclonal anti-HA Agarose	Thermo Fisher Scientific	Cat#: 26181; RRID: AB_2537081
Mouse monoclonal anti-Myc beads	Thermo Fisher Scientific	Cat#: 20169; RRID: AB_2537081
Flour-594 conjugated α-Bungarotoxin	Thermo Fisher Scientific	Cat #: B13423
Chemicals, peptides, and recombinant proteins		
Agrin	R and D Systems	Cat#: 550-AG-100
Rapsyn-EGFP (Rapsyn: aa 1M-412V, UniProt: P12672)	This paper	N/A (Custom-made)
Rapsyn (aa 1M-412V, UniProt: P12672)	This paper	N/A (Custom-made)
Rapsyn TPR1-2-EGFP (TPR1-2: aa 1M-76L. Uniprot: P12672)	This paper	N/A (Custom-made)
Rapsyn TPR 3-4-EGFP (TPR3-4: aa 77E-158D. UniProt: P12672)	This paper	N/A (Custom-made)
Rapsyn TPR 5-7-EGFP (TPR5-7: aa 159T-286V. UniProt: P12672)	This paper	N/A (Custom-made)
Rapsyn CC-RING-EGFP (TPR5-7: aa 296W-412V. UniProt: P12672)	This paper	N/A (Custom-made)
Rapsyn TPR1-4-EGFP (TPR1-4: aa 1M-158D. UniProt: P12672)	This paper	N/A (Custom-made)
Rapsyn TPR1-7-EGFP (TPR1-7: aa 1M-286V. UniProt: P12672)	This paper	N/A (Custom-made)
α-actinin2 (aa, 1M-894L, UniProt: Q9JI91)	This paper	N/A (Custom-made)
Calpain 2 (aa 1M-700L. UniProt: O085029)	This paper	N/A (Custom-made)
Actin, α1 (aa 1M-377F. UniProt: P68134)	This paper	N/A (Custom-made)
GST-AChR-α (aa 317N-428H UniProt: P04756)	This paper	N/A (Custom-made)
GST-AChR-β (aa 333H-469R. UniProt: P09690)	This paper	N/A (Custom-made)
GST-MACF1 (aa 1M-293I. UniProt: Q9QXZ0)	This paper	N/A (Custom-made)
GST-β-dystroglycan (aa 773Y-893P. UniProt: Q62165)	This paper	N/A (Custom-made)
Q3K-EGFP	This paper	N/A (Custom-made)
L14P-EGFP	This paper	N/A (Custom-made)
A73D-EGFP	This paper	N/A (Custom-made)
N88K-EGFP	This paper	N/A (Custom-made)
R91L-EGFP	This paper	N/A (Custom-made)
E147K-EGFP	This paper	N/A (Custom-made)

(*Continued on next page*)

Continued

REAGENT or RESOURCE	SOURCE	IDENTIFIER
R164H-EGFP	This paper	N/A (Custom-made)
L169P-EGFP	This paper	N/A (Custom-made)
R242W-EGFP	This paper	N/A (Custom-made)
L283P-EGFP	This paper	N/A (Custom-made)
L326P-EGFP	This paper	N/A (Custom-made)
C366A-EGFP	This paper	N/A (Custom-made)
1172del2-EGFP	This paper	N/A (Custom-made)
Y86F-EGFP	This paper	N/A (Custom-made)
EGFP	This paper	N/A (Custom-made)
Critical commercial assays		
Mix-n-Stain CF 633 Antibody Labeling Kit (50-100 μg)	Sigma	Cat#: MX633S100
Mix-n-Stain CF 555 Antibody Labeling Kit (50-100 μg)	Sigma	Cat#: MX555S100
Thrombin protease	Sigma	Cat#: GE27-0846-01
CK2 Kinase assay	New England Biolabs	Cat#: P6010S
Lambda protein phosphatase	New England Biolabs	Cat#: P0753S
Src Kinase assay	Cell signaling technology	Cat#: 7496
Experimental models: Cell lines		
HEK293T	ATCC	Cat#: CRL-3216; RRID: CVCL_0063
C2C12	ATCC	Cat#: CRL-1772; RRID: CVCL_0188
Rapsyn−/− myoblast	PMID: 10414969	N/A
Experimental models: Organisms/strains		
Rapsyn mutant mice (rapsyn −/−)	PMID: 7675108	N/A
R164H	This paper	N/A (Custom-made)
Recombinant DNA		
pGEX-6P-1	Sigma	Cat#: GE28-9546-48
pGEX-6P-1-AChR-α (aa 317-428)	This paper	N/A (Custom-made)
pGEX-6P-1-AChR-β (aa 333-469)	This paper	N/A (Custom-made)
pGEX-6P-1-MACF1 (aa 1-293)	This paper	N/A (Custom-made)
pGEX-6P-1-β-dystroglycan (aa 773-893)	This paper	N/A (Custom-made)
pEGX-6P-1-LRP4 (aa 1748-1905)	This paper	N/A (Custom-made)
pCDNA3.1-rapsyn	This paper	N/A (Custom-made)
pCDNA3.1-TPR1-2	This paper	N/A (Custom-made)
pCDNA3.1-TPR3-4	This paper	N/A (Custom-made)
pCDNA3.1-TPR5-7	This paper	N/A (Custom-made)
pCDNA3.1-TPR1-4	This paper	N/A (Custom-made)
pCDNA3.1-TPR1-7	This paper	N/A (Custom-made)
pCDNA3.1-CC-RING	This paper	N/A (Custom-made)
pCDNA3.1-TPR2-3	This paper	N/A (Custom-made)
pCDNA3.1-TPR4-5	This paper	N/A (Custom-made)
pCDNA3.1-TPR6-7	This paper	N/A (Custom-made)
pCDNA3.1-TPR5-6	This paper	N/A (Custom-made)
pEGFP-N1-rapsyn	This paper	N/A (Custom-made)
pEGFP-N1-TPR1-2	This paper	N/A (Custom-made)
pEGFP-N1-TPR3-4	This paper	N/A (Custom-made)
pEGFP-N1-TPR5-7	This paper	N/A (Custom-made)
pEGFP-N1-TPR1-4	This paper	N/A (Custom-made)
pEGFP-N1-TPR1-7	This paper	N/A (Custom-made)

(*Continued on next page*)

Continued

REAGENT or RESOURCE	SOURCE	IDENTIFIER
pEGFP-N1-CC-RING	This paper	N/A (Custom-made)
pEGFP-N1-TPR2-3	This paper	N/A (Custom-made)
pEGFP-N1-TPR4-5	This paper	N/A (Custom-made)
pEGFP-N1-TPR6-7	This paper	N/A (Custom-made)
pEGFP-N1-TPR5-6	This paper	N/A (Custom-made)
Software and algorithms		
ImageJ	National Institutes of Health	https://imagej.nih.gov/ij/download.html
Zen Software	Zeiss	https://www.zeiss.com/microscopy/us/products/microscope-software/zen-lite.html
Adobe illustrator	Adobe	https://www.adobe.com/products/illustrator/free-trial-download.html
Prism 7	GraphPad	https://www.graphpad.com/scientific-software/prism/

RESOURCE AVAILABILITY

Lead contact

Further information and requests for resources and reagents should be directed to and will be fulfilled by the lead contact, Lin Mei (lin.mei@case.edu).

Materials availability

All unique/stable reagents generated in this study are available from the lead contact with a completed Materials Transfer Agreement.

Data and code availability

The data supporting the current study are available from the Lead Contact on request. This study did not generate source code.

EXPERIMENTAL MODEL AND SUBJECT DETAILS

Mice

Rapsn null mutant mice were kindly provided by Dr. Peter Noakes (Gautam et al., 1995). The R164H mutant mice were generated by the transgenic and targeting facility of Case Western Reserve University using CRISPR-Cas9. Briefly, donor DNA, AGGCC CTGCG CTATG CCCAC AACAA CGATG ACACC ATGCT GGAGT GTCAC GTCTG CTGCA GCCTG GGCAG TTTCT ACGCC CAGGT CAAGG TGGGC CTGGT, was synthesized and PAGE purified by Integrated DNA Technologies. Cas9 protein (CP01-20) and sgRNA containing targeting sequence, TGCCC AGGCT GCAGC AGACA, were from PNA bio. Mixture containing Cas9 protein (100 ng / μl), sgRNA (50 ng / μl), and donor DNA (100 ng / μl) were injected into C57BL/6J fertilized eggs and the survival two-cell stage embryos were transferred to pseudo-pregnant C57BL/6J females. Mice carrying R164H mutation were screened by PCR analysis. Primers: 5′-ACA CCA TGC TGG AGT GCC GT −3′ and 5′- TTC TCA GGG AGC CTC AAA TC −3′ were used to verify WT genomic DNA, and primers: 5′- AGG CTG CAG CAG ACG TGA −3′ and 5′- ATG GGC AAT GCT TTC CTG GG −3′ were used to verify R164H mutant genomic DNA. Mice were housed in cages in a room with 12 hr light-dark cycle with *ad libitum* access to water and rodent chow diet (Diet P3000). Animal protocols have been approved by the Institutional Animal Care and Use Committee of Case Western Reserve University.

METHOD DETAILS

Protein expression, purification, and fluorescence labeling

Constructs for protein expression were generated through standard molecular cloning methods. Rapsn and truncation mutants, α-actinin, HSP90β, β-catenin, MACF1, actin, EGFP and calpain were cloned into modified pCDNA3.1 backbone containing Myc tag, His tag and a home-made thrombin digestion site, and transfected into HEK293T cells by polyethylenimine transfection (PEI, linear MW 25,000, Polysciences, Cat#: 23966-1) (Zhang et al., 2012, 2019). Three days after transfection, cells were harvested and sonicated in buffer containing 500 mM NaCl, 25 mM Tris, pH 7.4, 5 mM DTT, protease inhibitors (Complete EDTA-free, Sigma, Cat#: 11873580001), and phosphatase inhibitors (PhosSTOP, Sigma, Cat#: 4906845001). Lysates were centrifuged at 4°C, 14,000 x g for 30 min, and supernatants were collected and centrifuged again at 4°C, 14,000 x g for 30 min. They were incubated with Ni-NTA resins for 4 hr at 4°C; resins were washed with same buffer for three times and then incubated with the protease thrombin (working

condition: 1 U protease thrombin in 1 X cleavage buffer containing 20 mM sodium citrate, pH6.5, 20 mM NaCl, 0.01% PEG-8000, and 5% glycerol) to digest the tags and to elute conjugated proteins. Eluted proteins were further purified by size exclusion chromatography. For expression and purification of AChR-α, AChR-β, plectin1f, β-dys, respective cDNAs were cloned into pGEX-6P-1 vector with a GST tag. *Escherichia coli* BL21 cells were transformed with respective constructs and cultured in Lysogeny broth (LB) medium (supplied with ampicillin) at 18°C overnight. After the addition of 0.1 mM IPTG (final concentration) to induce protein expression, bacteria were cultured for another 9 hr, harvested and incubated with lysozyme in PBS for 20 min. Bacteria were lysed by sonication with 50% output and lysates were incubated with glutathione beads at 4°C for 1 hr. Beads were washed three times in PBS buffer and bound proteins were eluted by reduced glutathione and further purified by size exclusion chromatography in buffer containing 500 mM NaCl, 25 mM Tris (pH 7.4), and 5 mM DTT. Some proteins were labeled with CF555 tag using a kit (Mix-n-Stain CF 555, Sigma, MX555S100; Mix-n-Stain CF 633, Sigma, MX633S100) as described by the manufacturer.

Phase separation of proteins *in vitro* and imaging

Purified proteins were stored in high salt buffer (500 mM NaCl, 25 mM tris, pH 7.4, 5 mM DTT), and diluted into the physiological salt buffer (150 mM NaCl, 25 mM tris, pH 7.4, 5 mM DTT) to examine LLPS at room temperature. For co-condensation assay, 5 μM CF555 labeled cargo proteins were incubated with equimolar Rapsn-EGFP, and recruitment of cargo proteins was indicated by enrichment of CF555 signal into Rapsn droplets. For imaging droplets or condensates, diluted proteins were loaded on the glass bottom of culture dishes (35mm Dish, 14mm Glass diameter, uncoated; MatTek, P35G-1.5-14-C), and covered with a cover slide to reduce solution evaporation. Images were collected by confocal Zeiss LSM 810 using a 60 X oil objective.

Co-immunoprecipitation assay

The procedures for co-immunoprecipitation were performed as described previously (Zhang et al., 2008). Briefly, proteins were expressed in HEK293T cells by PEI transfection. 48 hr after transfection, cells were washed once with ice-cold PBS and lysed in buffer containing 5% glycerol, 150 mM NaCl, 25 mM Tris, pH7.4, 1% Triton X-100, protease inhibitors and phosphatase inhibitors. Lysates were centrifuged at 14,000 g for 20 min at 4°C, and the supernatants were incubated with beads overnight. Beads were pelleted by centrifugation at 4,000 x g for 1 min, 4°C, and washed with a buffer containing 5% glycerol, 150 mM NaCl, 25 mM Tris, pH7.4, 0.2% Triton X-100, protease inhibitors and phosphatase inhibitors for three times. Precipitated proteins were eluted by 1 X SDS boiling and detected by western blotting.

FRAP assay

Fluorescence signals were bleached using 100% intensity laser beam. Because fluorescence decays during image collection, two droplets or puncta were selected for single experiment. One was bleached and the other one was not bleached and acted as experimental controls. The ratio of bleached area / non-bleached control was calculated at different time points. The pre-bleach signal was normalized to 100%. For FRAP analysis of *in vitro* droplets, all data were collected with 20-40 min after proteins diluted in the physiological buffer to eliminate the possibility that aged droplets affect fluorescence recovery. For FRAP of AChR clusters in live muscles, muscles with tendons were isolated in oxygenated Ringer's solution (137 mM NaCl, 5 mM KCl, 12 mM $NaHCO_3$,1mM NaH_2PO_4,1mM $MgCl_2$, 2mM $CaCl_2$, 11 mM D-glucose, pH 7.3, perfused with 95% O_2 and 5% CO_2) and mounted on culture dishes with glass bottom for live imaging. FRAP assay was performed on Zeiss LSM 810 confocal.

Immunofluorescence staining

The procedures for immunostaining diaphragms were described previously (Xing et al., 2019; Zhao et al., 2018). Briefly, embryonic or P0 pups were sacrificed and fixed in 4% paraformaldehyde in PBS for 24 hr, and then diaphragms were dissected and rinsed in 0.1 M glycine in PBS for 1hr, room temperature, followed by three-time washing in 0.5% PBST (0.5% Triton X-100 in PBS). Samples were then blocked in the blocking buffer (5% BSA, 5% goat serum, 0.5% Triton X-100 in PBS) for 1 hr, room temperature, and incubated with primary antibodies diluted in blocking buffer, 4°C, overnight. Next day, samples were washed three times in washing buffer (0.5% Triton X-100 in PBS), and then incubated with fluorescence-labeled secondary antibodies and Flour-594 conjugated α-Bungarotoxin diluted in blocking buffer, room temperature, for 1-2 hr. After that, samples were washed and mounted with Vectashield mounting medium (H1000, Vector Laboratories, Burlingame, CA). Images were collected with LSM 810.

Live cell imaging and quantification of Rapsn-EGFP concentration in cells

For live cell imaging, HEK293T or C2C12 cells were cultured on 35mm dish with glass bottom plate (35 mm Dish, 14 mm Glass diameter, collagen coated; MatTek, P35GCOL-0-14-C), and transfected with Rapsn-EGFP or Rapsn-mCherry. For HEK293T cells, 12 hr after transfection, images were taken with confocal Zeiss LSM 810, supplemented with incubator with controllable temperature and CO_2 concentration (37°C, 5% CO_2). For C2C12 cells, after differentiation into myotubes, agrin was added to culture cells and images were taken simultaneously. To quantify Rapsn-EGFP concentration in HEK293T cells, the pixels of purified Rapsn-EGFP were calibrated using fluorescence microscopy and established the linear fitting of protein concentration and mean pixel intensity values. Occasionally, Rapsn became aggregated in ER or Golgi in proximal regions of nuclei. These aggregates were usually large and not associated to the plasma membrane. Cells with such aggregates were excluded from analysis. To avoid the potential impact of mitosis-associated cytoskeletal alteration on Rapsn LLPS, aggregates in mitotic cells were also excluded from analysis. Z stack

images were taken for all cells under same settings, and cell volumes were measured by imageJ plugins Volumest. The overall pixels were calculated by a sum-projection. The mean intensity was calculated as the ratio of overall pixel / cell volume.

Isolation of phase-separated condensates from aqueous phase

Proteins were stored in the buffer containing 500 mM NaCl, 25 mM tris, pH 7.4, 5 mM DTT, and pre-cleared via centrifugation at 14,000 x g for 1 min before using. To isolate phase-separated pellets with aqueous phase, proteins were diluted into low salt buffer (150 mM NaCl, 25 mM tris, pH 7.4, 5 mM DTT) with designed concentrations and combinations, and after incubation for 20 min at room temperature, samples were subjected to centrifugation at 14,000 x g for 15 min at room temperature. The aqueous phase/supernatant (designed as S) was transferred to a new tube and condensed phase/pellet were washed once with low salt buffer and re-suspended with half volume of supernatant fraction of high salt buffer (designed as P). Proteins in both S and P fractions were resolved by SDS-PAGE and analyzed by silver staining. Band intensities were quantified by ImageJ software.

Silver staining

The procedures for silver staining were performed as described previously (Shevchenko et al., 1996). Briefly, proteins were separated by SDS-PAGE (10% or 12%), and gels were fixed in solution containing 40% ethanol, 10% acetic acid in water for 30 min, and fixed gel was rinsed with 50% methanol for 10 min, followed by water washing for 10 min. The gel was then incubated with the sensitizing solution containing 0.02% $Na_2S_2O_3$ for 1 min, and rinsed in water for 2 X 1 min. Sensitized gel was then incubated in 0.1% silver nitrate solution for 20 min at 4°C. After that, gels were rinsed in water for 2 X 1 min and incubated in developing solution containing 2% Na_2CO_3 and 0.04% formalin to visualize protein bands.

CK2 and Src kinase assay

The procedures for CK2 and Src kinase assay were described by the manufacturers (CK2, New England Biolabs, Cat#: P6010S; Src, Cell signaling technology, Cat#: 7496).

Real time PCR

Total RNA was purified from mouse muscles using TRIzol (Thermo Fisher Scientific, 15596026) (Rio et al., 2010), and was measured and reverse transcribed to cDNAs according to manufacturer's protocol (Promega, GoScript reverse transcription kit, A2801) with Oligo dT primers. A 20 μL reaction system containing SYBR GreenER qPCR mix, gene-specific primers and cDNA was used to perform Real time PCR in StepOnePlus Real-Time PCR System (Thermo Fisher Scientific, 4376600) using 2hr cycling procedure, 95°C (10min), followed by 40 cycles of 95°C (15 s)- 60°C (60 s). Following primers were used. 5′-GGC AGG ACC AGA CAA AGC AA-3′ and 5′-CGAGTGAGCTGTTACCAAGCA-3′ for Rapsn; 5′-AAG GTC ATC CCA GAG CTG AA-3′ and 5′-CTG CTT CAC CAC CTT CTT GA-3′ for GAPDH.

QUANTIFICATION AND STATISTICAL ANALYSIS

Data were presented as mean ± SEM, unless otherwise indicated. Statistical analysis was performed by Unpaired Student t test, One-way ANOVA or Two-way ANOVA. Statistical difference was considered when $p < 0.05$.

Neuron, Volume *109*

Supplemental information

Membraneless condensates by Rapsn phase separation as a platform for neuromuscular junction formation

Guanglin Xing, Hongyang Jing, Zheng Yu, Peng Chen, Hongsheng Wang, Wen-Cheng Xiong, and Lin Mei

Supplemental Figures

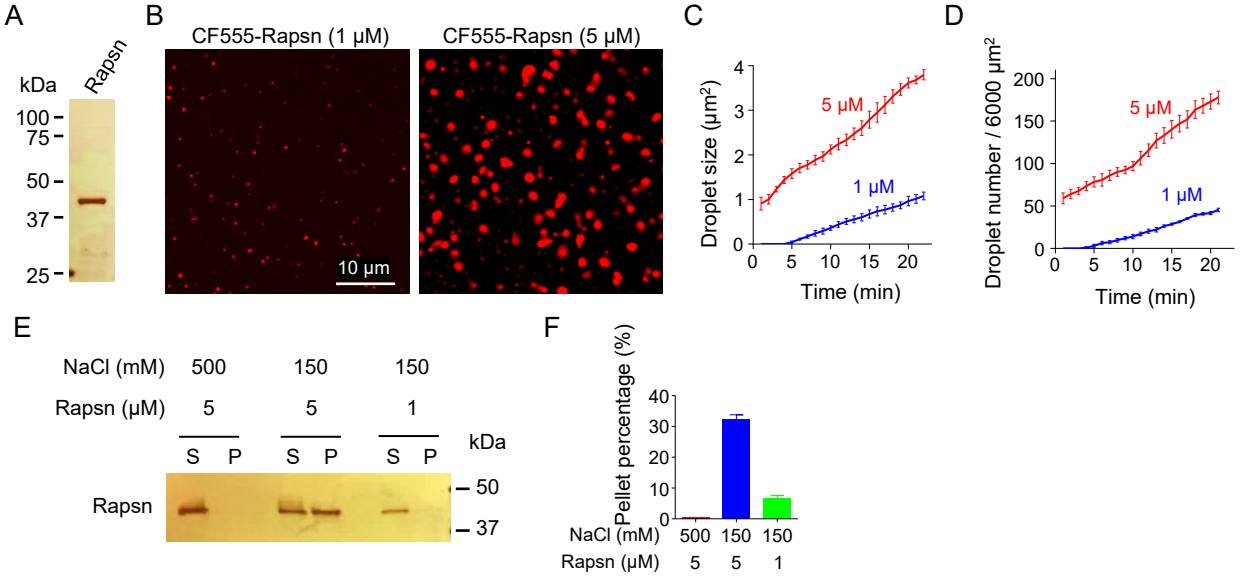

Figure S1. LLPS of Rapsn into condensates in vitro, Related to Figure 1.

(A) Silver staining showing purified Rapsn.
(B-D) Rapsn was able to phase separate into condensed droplets in a concentration-dependent manner.
(B) CF555-labeled Rapsn (1 μM and 5 μM) was able to phase separate into condensed droplets.
(C, D) Quantification of the droplet size and number formed by Rapsn (1 μM and 5 μM) at different time points. Data was shown as mean ± SEM; n = 3.
(E) Representative silver staining analysis showing the distribution of Rapsn in aqueous phase (S) and condensed phase (P) under different protein concentrations in the buffer containing 25 mM Tris, pH7.4, 5 mM DTT, and 150 mM NaCl or 500 mM NaCl.
(F) Quantification of percentage of Rapsn in pellets in (E). Data was shown as mean ± SEM; n = 3.

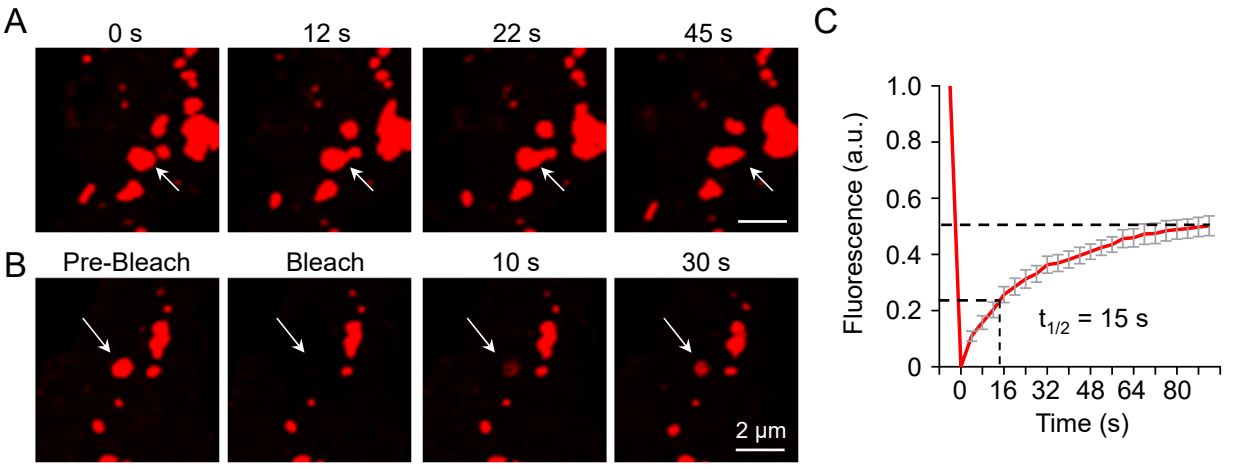

Figure S2. LLPS of Rapsn-mCherry into liquid-like compartments in HEK293T cells, Related to Figure 2.

(A) Fusion of two Rapsn-mCherry puncta in HEK293T cells.
(B) FRAP analysis showing dynamic exchange of Rapsn-mCherry between puncta and surrounding milieu.
(C) Quantification of fluorescence recovery in (B). Data were shown as mean ± SEM; n = 10.

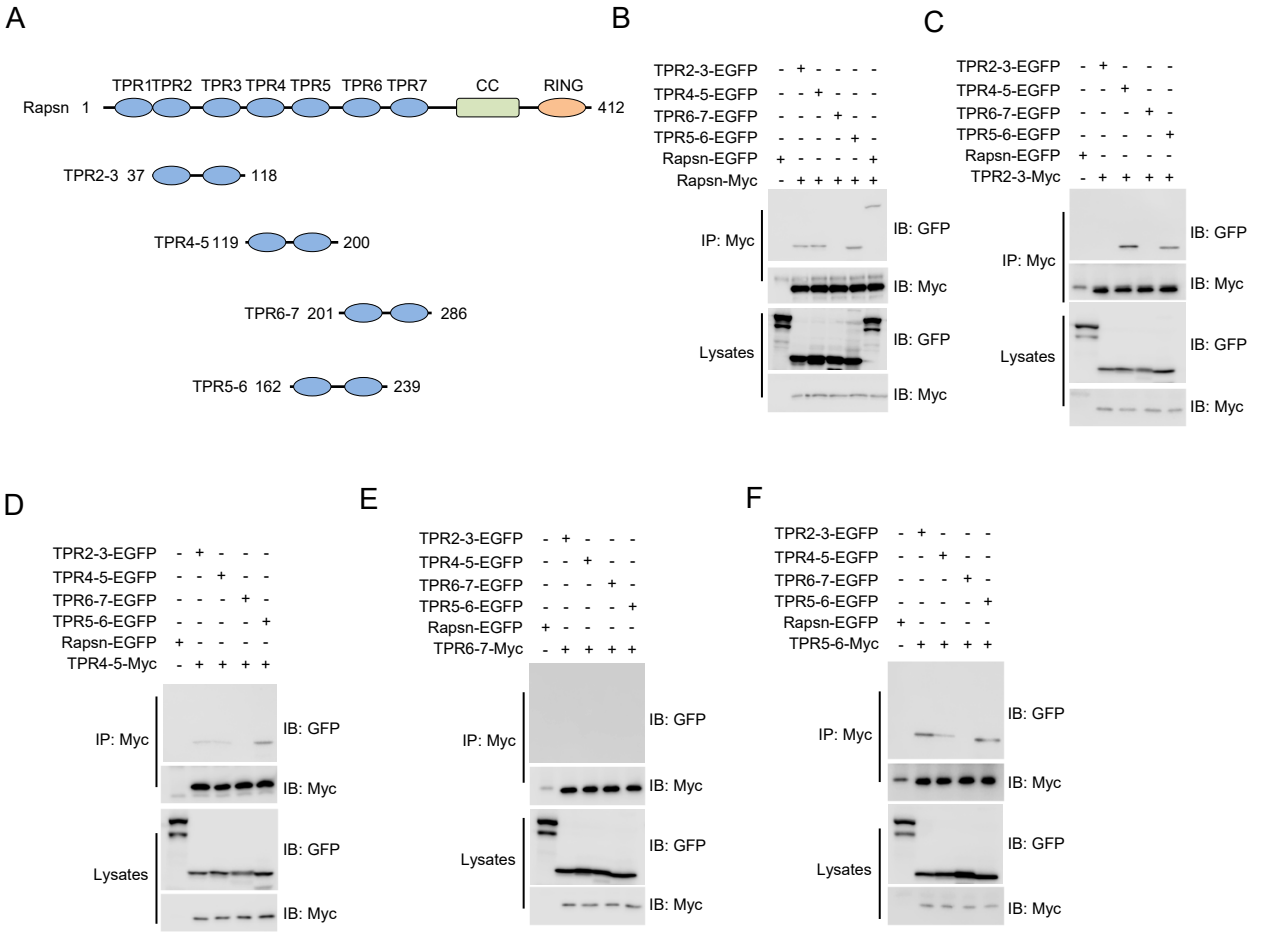

Figure S3. Multivalent binding of the TPR region, Related to Figure 4.

(A) Schematic diagram showing Rapsn domain structure, and various truncated proteins.
(B) Binding of Rapsn with TPR2-3, TPR4-5, TPR5-6, but not TPR6-7. EGFP-tagged TPR2-3, TPR4-5, TPR6-7, or TPR5-6 was cotransfected with Myc-tagged Rapsn into HEK293T cells. 48 hr later, cells were lysed and incubated with anti-Myc beads to precipitate Rapsn-Myc. Resulting complex was probed with indicated antibodies.
(C-F) TPR2-3, TPR4-5 or TPR5-6, but not TPR6-7 was able to bind with one another. The binding of TPR2-3-Myc (C), TPR4-5-Myc (D), TPR6-7-Myc (E), or TPR5-6-Myc (F) with EGFP-tagged TPR2-3, TPR4-5, TPR6-7, and TPR5-6 was characterized by co-immunoprecipitation.

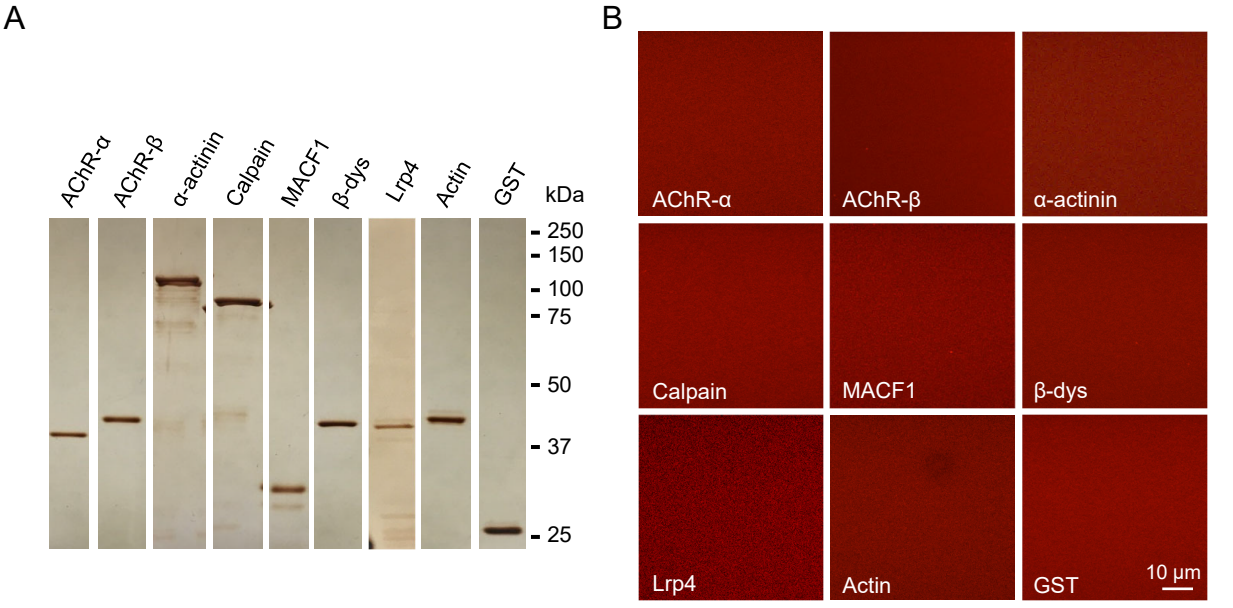

Figure S4. Failure of cargo proteins to phase separate into condensates by themselves, Related to Figure 5.

(A) Rapsn cargo proteins, as well as GST, Lrp4 and actin, were purified and examined by silver staining.
(B) Purified proteins were labeled with CF555, and their ability to form droplets was examined. Note that none of them was unable to phase separate into droplets.

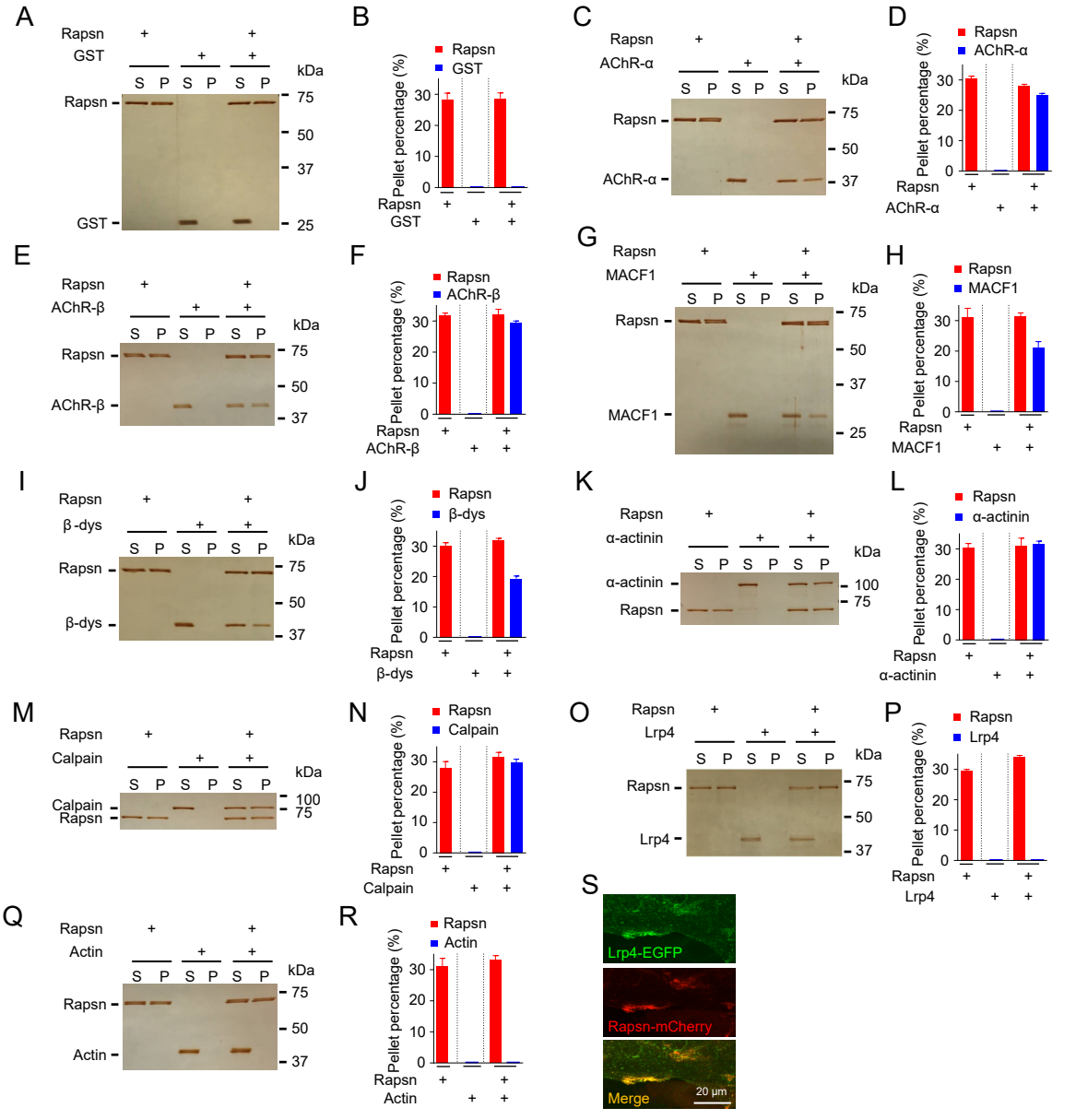

Figure S5. Recruitment of cargo proteins into Rapsn LLPS-mediated condensates, Related to Figure 5.

(A, B) GST was unable to be incorporated in Rapsn LLPS-mediated condensates.

(A) Representative silver staining image showing distribution of Rapsn-EGFP and GST in aqueous phase (S) and condensed phase (P) by Rapsn-EGFP (5 μM), GST (5 μM), or mixture containing Rapsn-EGFP (5 μM) and GST (5 μM). Note that GST was undetectable in pellets when examined alone or mixed with equimolar Rapsn-EGFP.

(B) Quantification of pellet percentage of Rapsn-EGFP and GST in different groups in (A). Data were shown as mean ± SEM; n = 3.

(C-R) AChR-α (C, D), AChR-β (E, F), MACF1 (G, H), β-dystroglycan (I, J), α-actinin (K, L) and calpain (M, N), were detectable in pellets when mixed with Rapsn-EGFP, but not alone. Lrp4 (O, P) or Actin (Q, R) was undetectable in pellets when examined alone or mixed with equimolar Rapsn-EGFP. Data were shown as mean ± SEM; n = 3.

(S) Colocalization of Lrp4-EGFP and Rapsn-mCherry in myotubes. Myoblasts were cotransfected with Lrp4-EGFP and Rapsn-mCherry. Resulting myotubes were treated with agrin for 12 hr and examined for co-distribution of Lrp4-EGFP and Rapsn-mCherry.

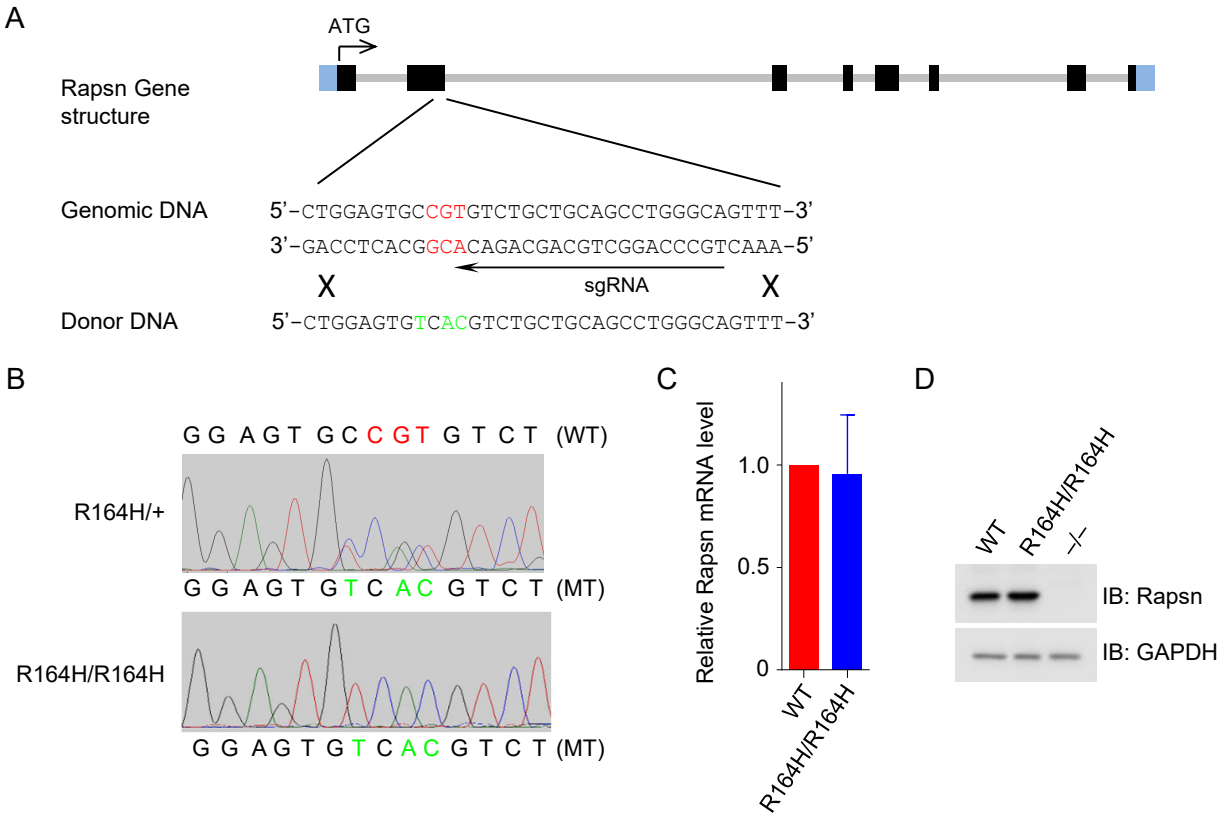

Figure S6. Generation of R164H knockin mutant mice by CRISPR-Cas9, Related to Figure 8.

(A) Generation of R164H knockin mutant mice by CRISPR-Cas9. Illustration of CRISPR-Cas9 strategy to generate R164H knockin mutant mice. The codon encoding R164 in genomic DNA was indicated in red. Mutated base pairs in donor DNA were indicated in green.

(B) Verification of R164H mutation by genomic DNA sequencing. Genomic DNA of indicated genotypes was sequenced. WT R164 was highlighted in red, and mutated base pairs were indicated in green.

(C) Comparable mRNA levels of Rapsn in WT and R164H/R164H mutant mice. Data were shown as mean ± SEM; n = 3, Student T-test.

(D) Similar Rapsn protein levels between WT and R164H/R164H mutant mice.

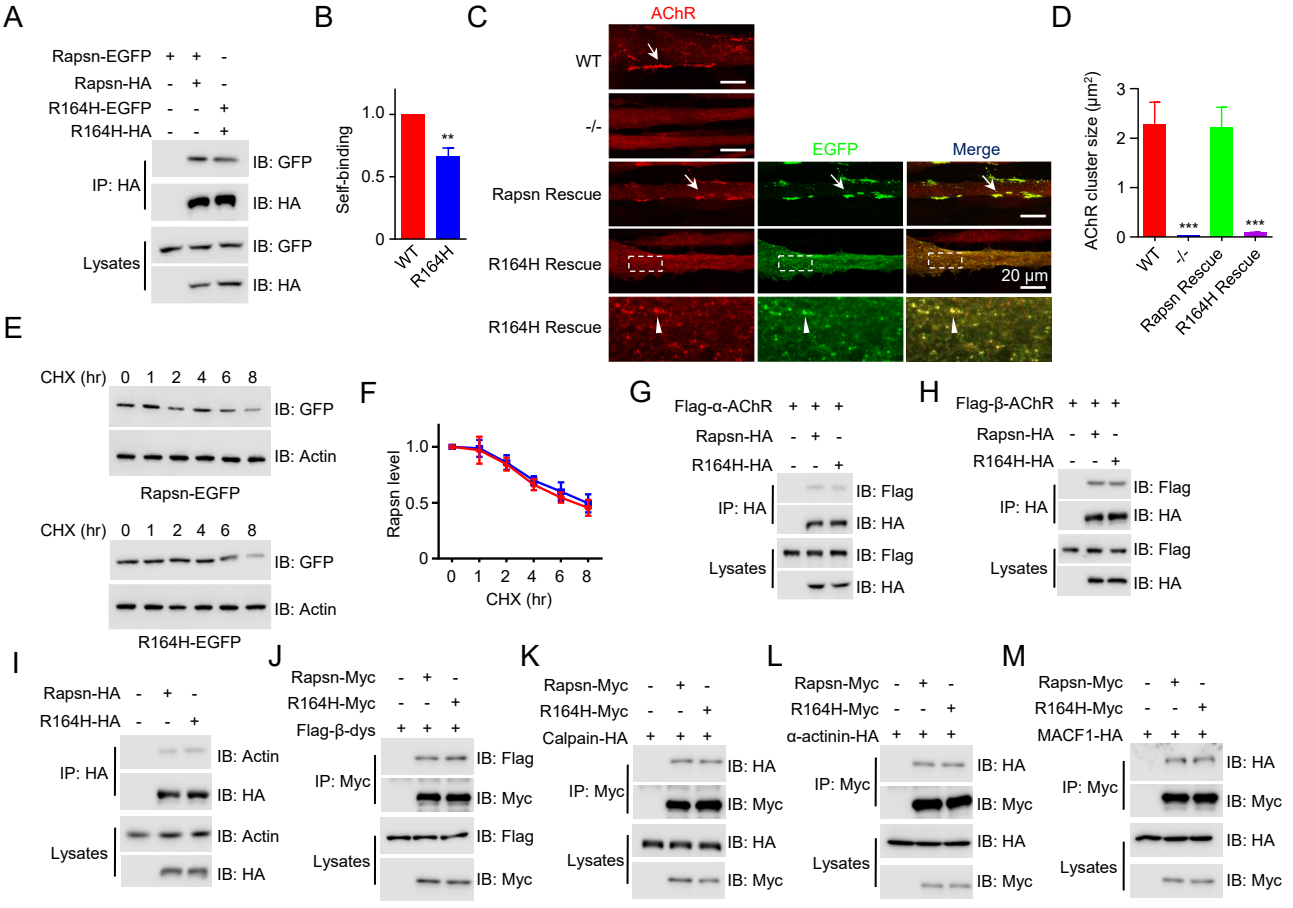

Figure S7. R164H is impaired in self-association and in rescuing AChR clustering in Rapsn -/- myotubes, Related to Figure 8.

(A, B) Reduced Rapsn self-association by R164H mutation. Data were shown as mean ± SEM; n = 3; **, P < 0.01; Student T-test.

(C, D) Failure of R164H mutant Rapsn in rescuing agrin-induced AChR clusters in Rapsn -/- myotubes.

(C) WT, Rapsn -/-, or Rapsn -/- myotubes transfected with EGFP-tagged WT or R164H mutant Rapsn was treated with agrin for 12 hr and stained with Flour 594-α-BTX (red) to label AChR clusters. Arrows, large AChR or Rapsn-EGFP clusters; arrow heads, small AChR or R164H-EGFP clusters.

(D) Quantification of AChR cluster size in (C). Clusters (> 0.01 μm2) identifiable by ImageJ were quantified. Data were shown as mean ± SEM; n = 3; ***, P < 0.001; One-way ANOVA.

(E, F) Comparable degradation of WT and R164H mutant Rapsn in HEK293T cells. HEK293T cells were transfected with EGFP-tagged WT or R164H mutant Rapsn. After 12 hr, cells were separated into 6-well plates and cultured for additional 12 hr. Cells were treated with CHX (50 μM) for indicated times; resulting lysates were blotted with anti-GFP antibody. (F) Quantitative data in (E). Data were shown as mean ± SEM; n = 3; Student T-test.

(G, H) Comparable interaction of WT and R164H mutant Rapsn with AChR subunits examined by co-immunoprecipitation assay.

(I) Comparable binding of WT or R164H mutant Rapsn with actin. HA-tagged WT or R164H mutant Rapsn was transfected into myoblasts. Resulting myotubes were lysed and the interaction of Rapsn and actin was examined by co-immunoprecipitation assay.

(J-M) Comparable binding of WT and R164H Rapsn with β-dystroglycan (J), calpain (K), α-actinin (L), or MACF1 (M) examined by co-immunoprecipitation.

Supplmental Table

Table S1. Effects of CMS mutations on Rapsn LLPS and co-condensation with cargo proteins, Related to Figure 7.

CMS mutations	LLPS	Co-condensation					
		AChR-α	AChR-β	MACF1	β-dys	α-actinin	Calpain
Q3K	-	-	-	-	-	-	-
L14P	↓	NA	NA	NA	NA	NA	NA
A73D	-	-	-	-	-	-	-
N88K	↓	NA	NA	NA	NA	NA	NA
R91L	-	-	-	-	-	-	-
A142D	-	-	-	-	-	-	-
E147K	-	-	-	↓	-	-	-
R164H	↓	NA	NA	NA	NA	NA	NA
L169P	-	-	-	-	-	-	-
R242W	-	-	-	-	-	-	-
L283P	-	-	-	-	-	-	-
L326P	-	↓	↓	-	-	-	-
C366A	-	-	-	-	-	-	-
1177del2	-	-	-	-	↓	-	-

"↓", reduced; "-", no effect; "NA", not applicable